Supporting Information

Size-dependent properties and unusual reactivity of novel nonplanar heterocycloarenes

Jiangyu Zhu,[a] Wenhao Li,[a] Ning Zhang,[a] Dongyue An,[a] Yan Zhao,[a] Xuefeng Lu,*[,a] and Yunqi Liu*[,a]

[a]Department of Materials Science, Fudan University, Shanghai 200433, China.

*E-mail: luxf@fudan.edu.cn; liuyq@fudan.edu.cn

Table of Contents

1. Experimental Section

1.1 General

Unless special mention, all the chemicals and reagents were purchased from commercial sources and used without further purification. Anhydrous THF were distilled from sodium-benzophenone immediately prior to use. Precursors **1**[1] and **2**[2] were prepared according to literature procedures. All the reactions and manipulations under nitrogen were by using standard inert atmosphere and Schlenk techniques.

The ^{1}H NMR and ^{13}C NMR spectra were recorded in solution of $CDCl_3/CD_2Cl_2$ on a Varian Mercury Plus-400 spectrometer, with tetramethylsilane (TMS) as the internal standard. The splitting patterns are designated as follows: s (singlet); d (doublet); t (triplet); and m (multiplet). 2D NOESY NMR spectra were measured on a Bruker AVANCE III HD spectrometer. High resolution mass spectroscopies (HRMS) were recorded on a Thermo Scientific Q Exactive hybrid quadrupole-Orbitrap mass spectrometer, equipped with atmospheric pressure chemical ionization (APCI) source. MALDI-TOF mass spectra (MS) were recorded on a Bruker amazon instrument. Ultraviolet-visible (UV-vis) absorption spectra were measured on a PerkinElmer Lambda-750 spectrophotometer. Fluorescence spectra were recorded on an Edinburgh fluorescence spectrometer. Quantum yield were calculated using the quinine sulfate in 0.1 mol/L H_2SO_4-toluene (QY = 54%) as standard, with an absorbance less than 0.05 at 350 nm as a reference. The electrochemical measurements were carried out in anhydrous DCM with 0.1 M tetrabutylammonium hexafluorophosphate (n-Bu_4NPF_6) as the supporting electrolyte at room temperature under the protection of nitrogen. A glass carbon disk was used as working electrode, a platinum wire was used as counting electrode, and Ag/Ag^+ electrode as reference electrode. Redox couple ferrocenium/ferrocene was used as an internal standard.

1.2 Synthetic procedures and characterization data

Synthesis of macrocycles 3a and 3b by Suzuki coupling reaction.

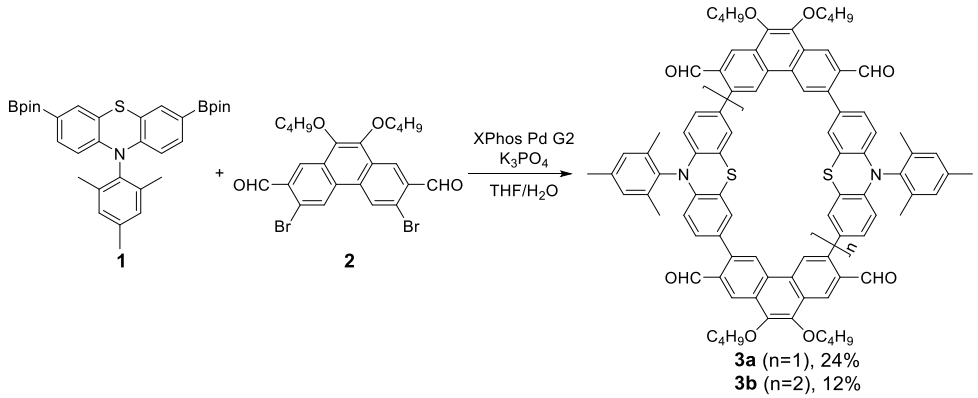

Compound **1**[1] was prepared according to literature procedure. Compound **2**[2] was synthesized similarly according to literature procedure. Under a nitrogen atmosphere, **1** (212 mg, 373 μmol), **2** (200 mg, 373 μmol), XPdos Pd G2 (50 mg, 63.5 μmol) and THF (200 mL) were carefully degassed before K_3PO_4 (12.8 g) dissolved in deionized water (200 mL) was addin g. The mixture was stirred at 55 ºC for 24h. After been cooled to room temperature, the organic solvent was removed under reduced pressure, then H_2O and DCM were added. The organic layer was separated, dried over anhydrous $MgSO_4$, filtered and concentrated to afford the crude product, which was purified by column chromatography (silica gel, DCM/petroleum ether/ethyl acetate = 5:1:0.6) to remove catalysts. And then further purified by preparative GPC using $CHCl_3$ at a rate of 16 mL/min. Orange solid macrocycle **3a** was obtained in 24% yield (60 mg). ^{1}H NMR (400 MHz, $CDCl_3$) δ 10.21 (s, 4H), 8.89 (s, 4H), 8.72 (s, 4H), 7.50 (s, 4H), 7.14 (s, 4H), 6.80 (d, J = 8.2 Hz, 4H), 6.14 (d, J = 8.3 Hz, 4H), 4.27 (d, J = 6.6 Hz, 8H), 2.41 (s, 6H), 2.27 (s, 12H), 1.92 (dd, J = 14.2, 6.7 Hz, 8H), 1.67 – 1.61 (m, 8H), 1.04 (t, J = 7.3 Hz, 12H). ^{13}C NMR (101 MHz, $CDCl_3$) δ 192.24, 144.16, 142.29, 140.30, 139.12, 134.32, 132.87, 132.77, 132.61, 131.55, 131.26, 130.82, 130.29, 127.36, 125.82, 124.13, 119.88, 114.22, 73.96, 32.66, 29.93, 19.62, 18.21, 14.21. HRMS (APCI, m/z): [M] calcd for $C_{90}H_{82}N_2O_8S_2$, 1383.5585; found, 1383.5551. Orange solid macrocycle **3b** was obtained in 12% yield (30 mg). ^{1}H NMR (400 MHz, $CDCl_3$) δ 10.19 (s, 6H), 8.88 (s, 6H), 8.59 (s, 6H), 7.13 (s, 6H), 7.02 (s, 6H), 6.87 (d, J = 8.5 Hz, 6H), 6.04 (d, J = 8.4 Hz, 6H), 4.27 (t, J = 6.6 Hz, 12H), 2.39 (s, 9H), 2.31 (s, 18H), 1.98 – 1.88 (m,

12H), 1.62 (dd, J = 14.9, 7.4 Hz, 12H), 1.04 (t, J = 7.3 Hz, 18H). ^{13}C NMR (101 MHz, $CDCl_3$) δ 192.36, 144.12, 141.10, 140.88, 139.02, 137.96, 134.41, 133.18, 132.31, 131.17, 130.82, 130.45, 129.86, 127.82, 125.67, 123.74, 118.73, 114.24, 73.97, 32.64, 21.41, 19.62, 18.28, 14.22. HRMS (APCI, m/z): [M] calcd for $C_{135}H_{123}N_3O_{12}S_3$, 2074.8342; found, 2074.8281.

Synthesis of compound 4a.

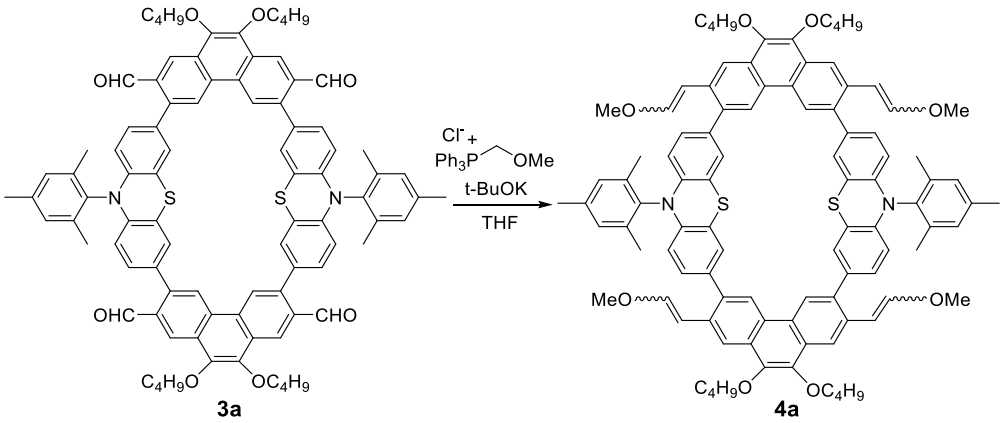

Under nitrogen atmosphere, to 100 mL Schlenk flask were added a solution of methoxymethyltriphenyl-phosphonium chloride (686mg, 2.67 mmol) in anhydrous THF (30 mL) at 0 ºC was added t-BuOK (2 mL, 2M in THF). After stirring for 30 mins, the solution of **3a** (30 mg, 22 μmol) in anhydrous THF (20mL) was added and stirred at room temperature for overnight. The reaction solution was quenched by brine and extracted by DCM. The organic layer was separated, dried over anhydrous $MgSO_4$, filtered and concentrated to afford the crude product, which was purified by flash column chromatography (silica gel, DCM/petroleum ether = 1:1). Yellow solid precursor **4a** was obtained in 86% yield (28 mg). ^{1}H NMR (400 MHz, $CDCl_3$) δ 8.93 (s, 1H), 8.42 (s, 2H), 8.16 (s, 2H), 7.12 (s, 2H), 7.05 (s, 1H), 7.02 (s, 1H), 6.94 (d, J = 8.1 Hz, 2H), 6.16 (d, J = 7.7 Hz, 1H), 6.01 (s, 2H), 5.98 (s, 1H), 5.40 (d, J = 7.2 Hz, 1H), 4.24 (d, J = 5.8 Hz, 4H), 3.82 (s, 3H), 3.62 (s, 3H), 2.40 (s, 3H), 2.26 (s, 6H), 1.91 (d, J = 6.5 Hz, 4H), 1.64 (d, J = 7.7 Hz, 4H), 1.05 (s, 6H). ^{13}C NMR (101 MHz, $CDCl_3$) δ 149.39, 148.50, 143.69, 143.24, 143.13, 141.31, 138.48, 137.34, 136.04, 135.00, 132.83, 131.56, 130.52, 129.71, 128.85, 127.96, 127.20, 126.77, 124.16, 123.72,

122.94, 118.74, 118.20, 113.39, 113.28, 105.40, 104.13, 73.50, 60.93, 57.23, 33.00, 32.84, 31.75, 30.38, 29.94, 21.40, 19.78, 18.30, 14.29. HRMS (APCI, m/z): [M] calcd for $C_{98}H_{98}N_2O_8S_2$, 1495.6837; found, 1495.6809.

Synthesis of compound 4b.

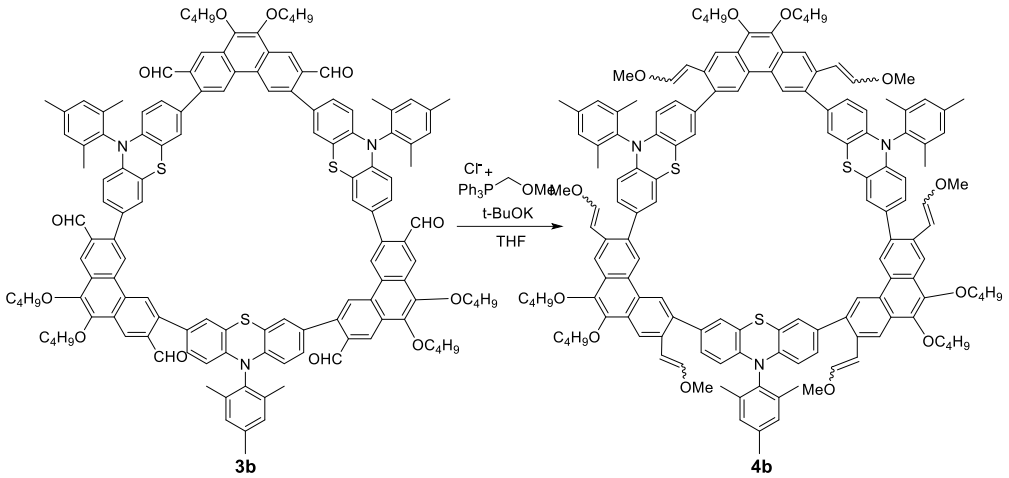

The synthesis of the compound **4b** was same as the procedure of compound **4a**. Yellow solid precursor **4b** was obtained in 89% yield (29 mg). ^{1}H NMR (400 MHz, CD_2Cl_2) δ 8.91 (s, 1H), 8.35 (s, 2H), 8.17 (s, 2H), 7.14 (s, 1H), 7.08 (d, J = 12.8 Hz, 2H), 7.02 (s, 1H), 6.97 (s, 1H), 6.87 (d, J = 12.5 Hz, 2H), 6.27 (d, J = 7.2 Hz, 1H), 5.97 (s, 2H), 5.37 (d, J = 7.3 Hz, 1H), 4.24 (s, 4H), 3.86 (s, 3H), 3.66 (s, 3H), 2.38 (s, 3H), 2.29 (s, 6H), 1.93 (d, J = 6.8 Hz, 4H), 1.65 (d, J = 7.3 Hz, 4H), 1.06 (d, J = 6.5 Hz, 6H). ^{13}C NMR (101 MHz, CD_2Cl_2) δ 149.72, 148.95, 143.20, 138.70, 138.14, 134.94, 130.53, 129.12, 127.53, 126.87, 123.83, 122.72, 117.85, 113.90, 104.80, 103.41, 73.44, 60.98, 57.05, 32.94, 32.81, 29.92, 21.08, 19.77, 17.92, 14.14, 14.04. HRMS (APCI, m/z): [M] calcd for $C_{147}H_{147}N_3O_{12}S_3$, 2243.0220; found, 2243.0098.

Synthesis of phenothiazine-containing heteroarene PTZ1.

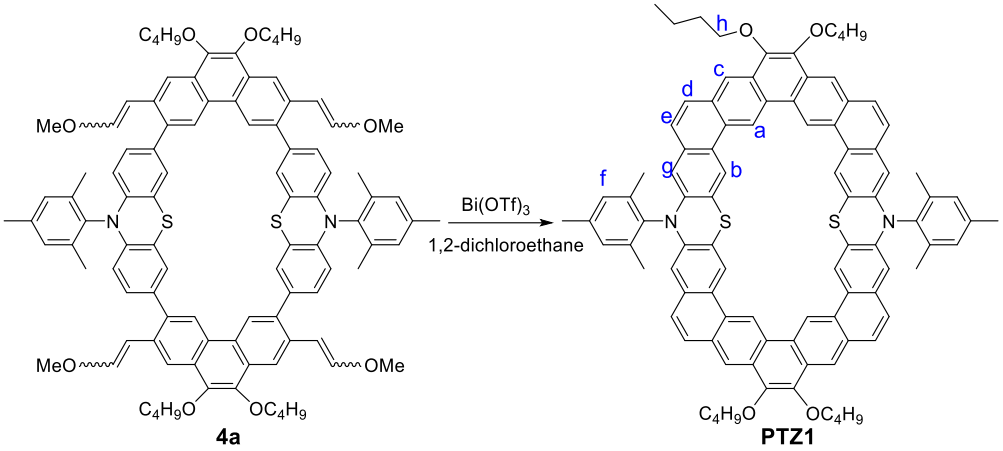

Under nitrogen atmosphere, compound **4a** (28 mg, 19 μmol), $Bi(OTf)_3$ (25 mg, 38 μmol) and 30 mL dry 1,2-dichloroethane were added in 100 mL flask, and the solution was stirred at room temperature for 3h. The reaction solvent was removed under reduce pressure. The residue was purified by flash column chromatography (silica gel, DCM/petroleum ether = 1:1). Yellow solid phenothiazine-containing heterocycloarene **PTZ1** was obtained in 86% yield (22 mg). 1H NMR (400 MHz, $CDCl_3$) δ 10.30 (s, 4H), 9.16 (s, 4H), 8.54 (s, 4H), 7.78 (d, J = 9.1 Hz, 4H), 7.45 (d, J = 9.0 Hz, 4H), 7.28 (s, 4H), 6.57 (s, 4H), 4.33 (t, J = 6.7 Hz, 8H), 2.55 (s, 6H), 2.31 (s, 12H), 2.02 – 1.94 (m, 8H), 1.68 (dq, J = 14.7, 7.4 Hz, 8H), 1.07 (t, J = 7.4 Hz, 12H). ^{13}C NMR (101 MHz, $CDCl_3$) δ 147.31, 143.25, 138.89, 132.28, 130.84, 130.41, 128.85, 128.14, 127.79, 127.34, 126.99, 124.71, 124.22, 122.26, 121.27, 119.32, 116.52, 111.45, 73.53, 32.94, 31.69, 19.79, 18.44, 14.34. HRMS (APCI, m/z): [M] calcd for $C_{94}H_{82}N_2O_4S_2$, 1367.5789; found, 1367.5758.

Synthesis of phenothiazine-containing heteroarene PTZ2.

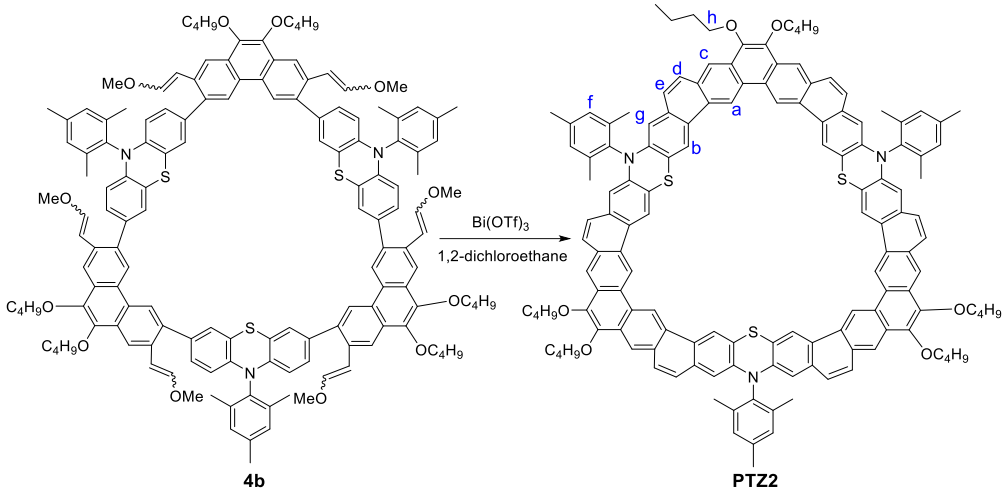

The synthesis of heterocycloarene **PTZ2** was same as the procedure of compound **PTZ1**. Yellow solid **PTZ2** was obtained in 79% yield (21 mg). ^{1}H NMR (400 MHz, CD_2Cl_2) δ 9.72 (s, 6H), 8.76 (s, 6H), 8.57 (s, 6H), 7.73 (d, J = 8.9 Hz, 6H), 7.37 (d, J = 8.9 Hz, 6H), 7.24 (s, 6H), 6.60 (s, 6H), 4.32 (t, J = 6.6 Hz, 12H), 2.48 (s, 9H), 2.32 (s, 18H), 2.01 – 1.92 (m, 12H), 1.66 (dd, J = 14.3, 6.8 Hz, 12H), 1.06 (t, J = 7.4 Hz, 18H). ^{13}C NMR (101 MHz, $CDCl_3$) δ 142.16, 140.30, 138.68, 138.37, 135.42, 132.64, 130.78, 130.70, 128.90, 128.75, 128.58, 127.13, 126.87, 121.82, 121.36, 117.39, 112.82, 73.47, 32.86, 21.50, 19.74, 18.59. HRMS (APCI, m/z): [(M+H)$^{+}$] calcd for $C_{141}H_{123}N_3O_6S_3$, 2051.8680; found, 2051.8604.

Synthesis of compound PTZ1-Oxi.

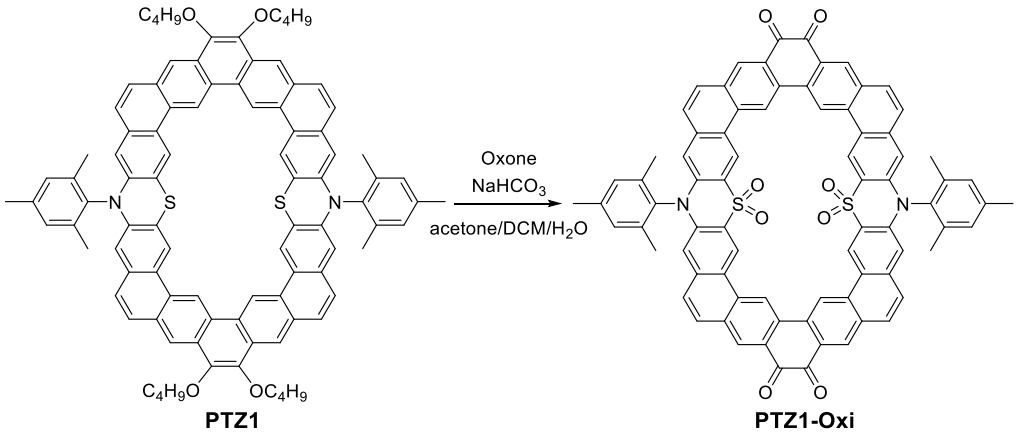

The compound **PTZ1-Oxi** was synthesized similarly to literature procedure.[3] To a solution of heterocycloarene **PTZ1** (30 mg, 21 μmol) in acetone/DCM/H_2O (3 mL:3

mL;3 mL) was added Oxone (298 mg, 971 μmol) and $NaHCO_3$ (582 mg, 6.93 mmol). The reaction mixture was stirred at room temperature for overnight. The reaction solution was quenched by $NaHSO_3$ solution, and extracted by DCM. After removal of the solvent under reduced pressure, the residue was purified by recrystallizing from a mixed solution of $CHCl_3/CH_3OH$ to afford the desired orange product **PTZ1-Oxi**. The isolated yield: 15% (4.0 mg). ^{1}H NMR (400 MHz, $CDCl_3$) δ 10.28 (s, 4H), 9.97 (s, 4H), 8.80 (s, 4H), 7.89 (d, J = 9.1 Hz, 4H), 7.65 (d, J = 9.0 Hz, 4H), 7.33 (s, 4H), 7.09 (s, 4H), 2.58 (s, 6H), 2.11 (s, 12H). MALDI-TOF Mass: *m/z* 1203.2, calc. 1202.3.

1.3 OFET fabrication and characterization

The SiO_2/Si wafers were first washed with deionized water, hot piranha solution (H_2SO_4/H_2O_2 = 2:1), deionized water, ethanol in sequence, and finally were dried in an oven at 70°C. For the surface modification, a small drop of octadecyltrichlorosilane (OTS) surrounded by those cleaned SiO2/Si substrates were put into a Petri dish. Then the dish was placed into a vacuum oven and kept at 120°C for 3 hours. After cooling to room temperature, OTS self-assembled monolayer was formed on the surface of the SiO_2/Si wafers. Those OTS modified wafers should be washed immediately in turn by hexane, ethanol, and chloroform and finally were blown dry with high-purity nitrogen gas.

Bottom-gate and bottom-contact (BGBT) configuration OTFTs were fabricated by spin-coating on the OTS modified Si/SiO_2 substrate. Gold source/drain electrodes were prepared by vacuum deposition through shadow mask to give a defined channel length (L = 10 μm) and channel width (W = 1.4 mm). The **PTZ1** dissolved in chloroform was spun with speed of 3000 rpm for 60 seconds. OTFT devices were measured under glovebox with Keysight 4200. Saturation mobilities were calculated according to the equation.

$$I_{DS} = \frac{W}{2L} C_i \mu (V_{GS} - V_T)^2$$

where I_{DS} is the drain-source current, μ is the field-effect mobility, V_G is the gate voltage, V_T is the threshold voltage, W is the channel width, L is the channel width length, C_i is

the capacitance of the insulating layer. In this work, the 300 nm SiO_2 surface layer with the capacitance of 11nF cm^{-2} was employed as the dielectric. OFET characteristics were obtained by applying a gate voltage from −60 V to 10 V, with the drain-source voltage kept at −60 V.

2. Additional spectra

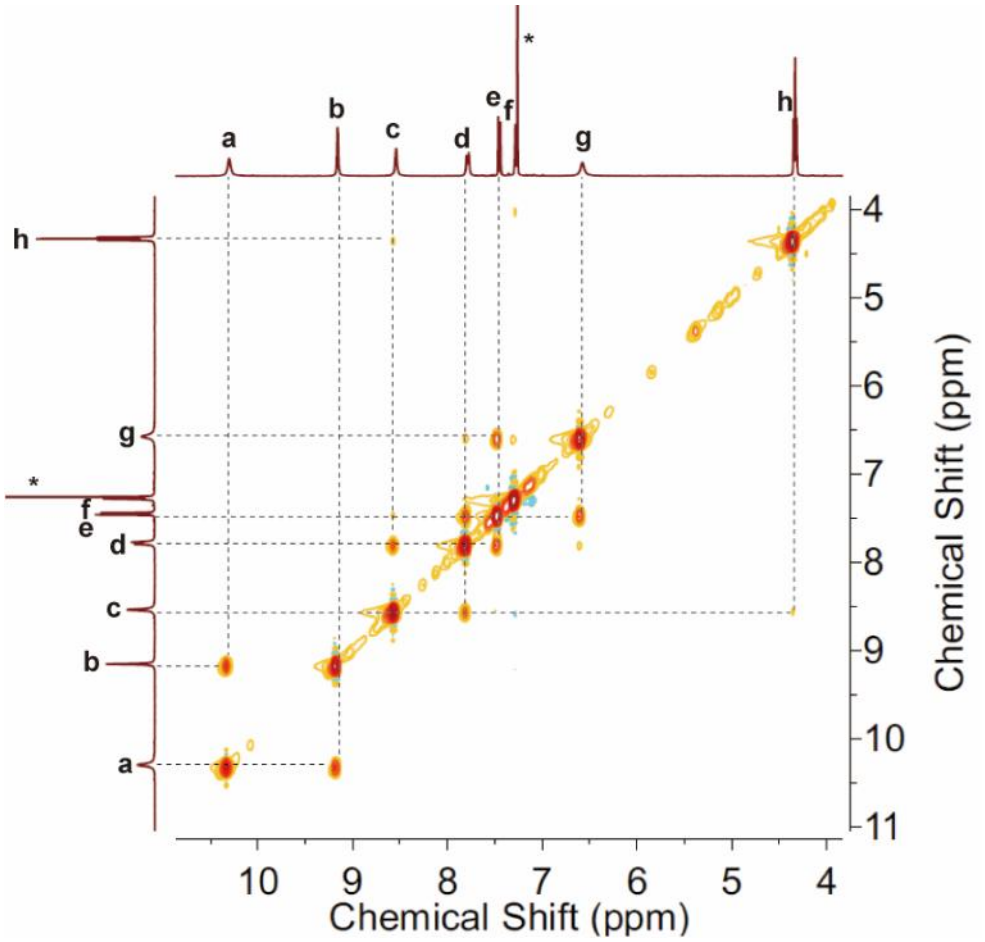

Figure S1. 2D NMR NOESY spectra of **PTZ1** in $CDCl_3$ (500 MHz).

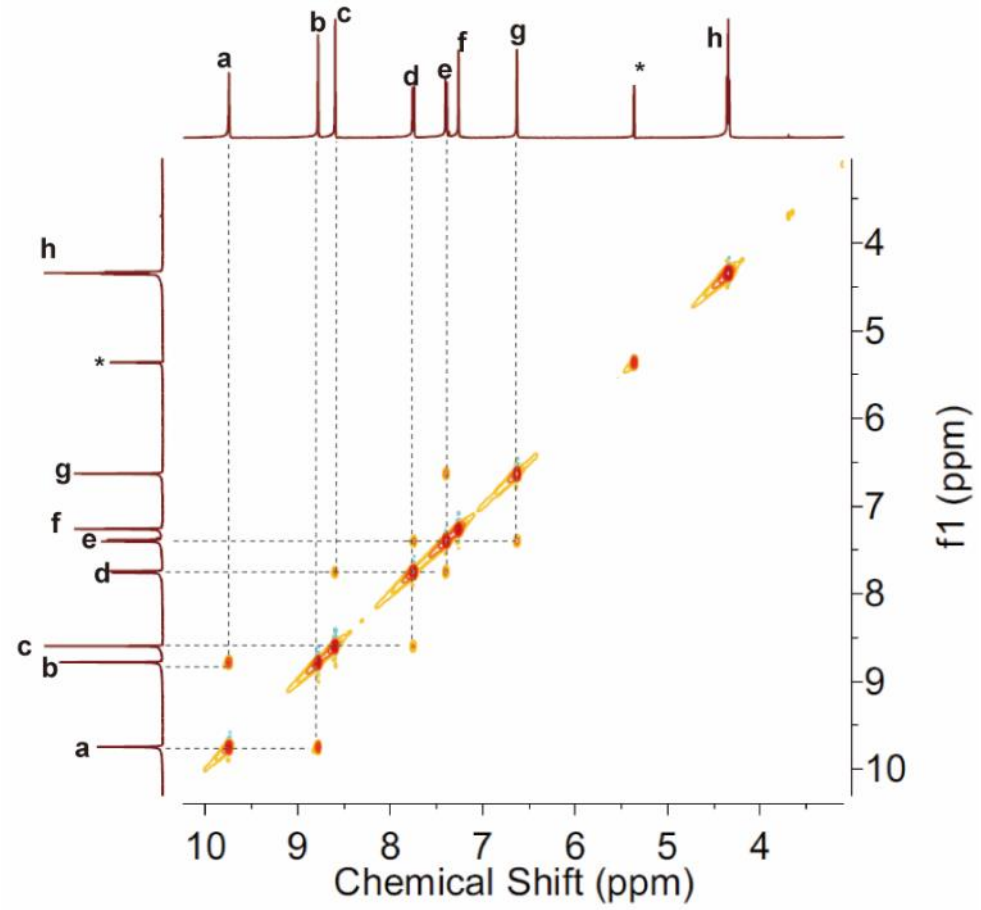

Figure S2. 2D NMR NOESY spectra of **PTZ2** in CD_2Cl_2 (500 MHz).

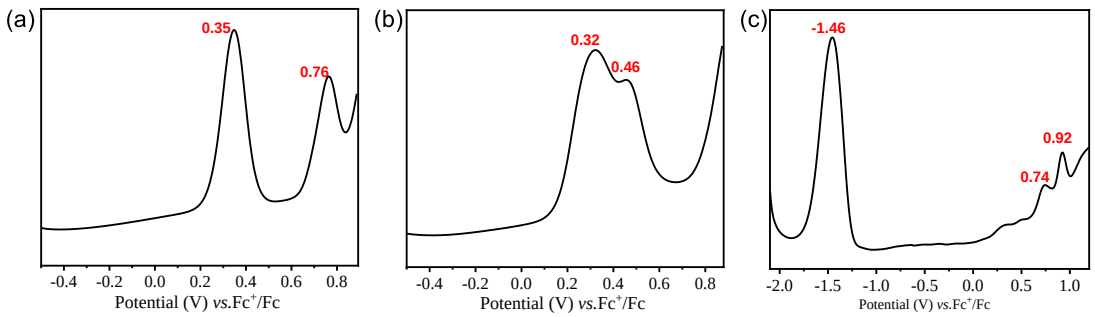

Figure S3. Differential pulse voltammograms (DPV) of (a)**PTZ1**, (b)**PTZ2** and (c)**PTZ1-Oxi** in DCM solutions.

Table S1. Energy level data of **PTZ1**, **PTZ2** and **PTZ1-Oxi**.

Comp.	λ_{onset} (nm)[a]	E_g (eV)[b]	E_{ox}^{onset} (V)[c]	E_{HOMO} (eV)[d]	E_{LUMO} (eV)[e]
PTZ1	477	2.60	0.29	-5.09	-2.49
PTZ2	483	2.57	0.14	-4.94	-2.37
PTZ1-Oxi	545	2.28	0.69	-5.49	-3.21

[a] Onset absorption wavelength. [b] Optical band gap. [c] Onset oxidation potential. [d] Calculated from E_{ox}^{onset}. E_{HOMO} = -(E_{ox}^{onset} + 4.80) eV. [e] E_{LUMO} = E_g + E_{HOMO}.

Fullerene binding NMR studies[4-5]

The host molecule solution of N,S-heterocycloarenes (0.92 mM, CD_2Cl_2) were titrated in an NMR tube sealed with a plastic stopper, by adding known quantities (2 μL) of a stock solution of fullerene (C_{60} or C_{70}) in CS_2. After each addition, the NMR tube was quickly shaken to ensure good mixing of the solutions and then the spectra were recoded. The dilution effect can be ignored during titration to add little enough fullerene solution to the system.

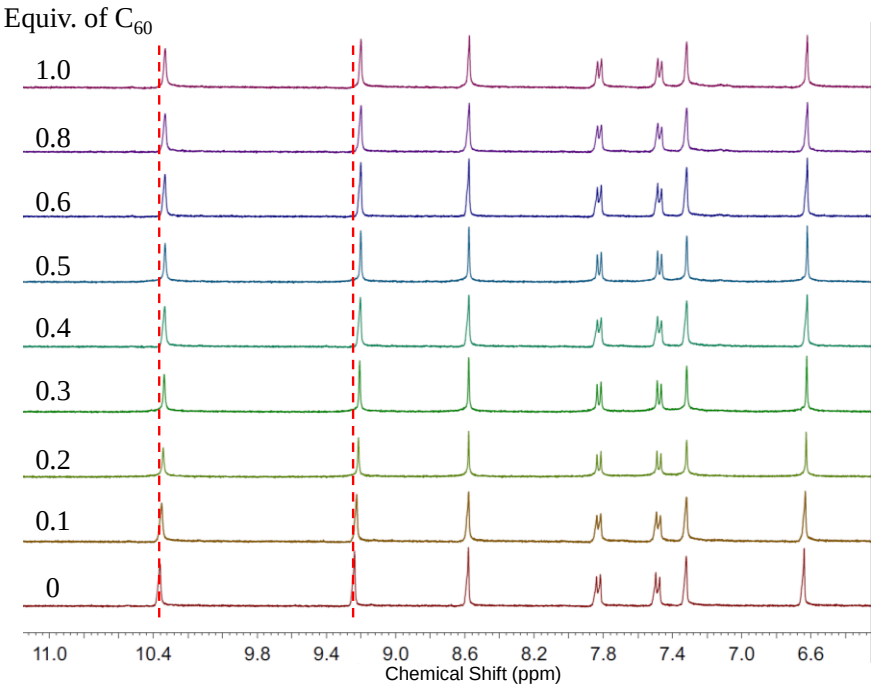

Figure S4. Partial ^{1}H NMR (400 MHz, CD_2Cl_2) spectra for titration of **PTZ1** with C_{60}.

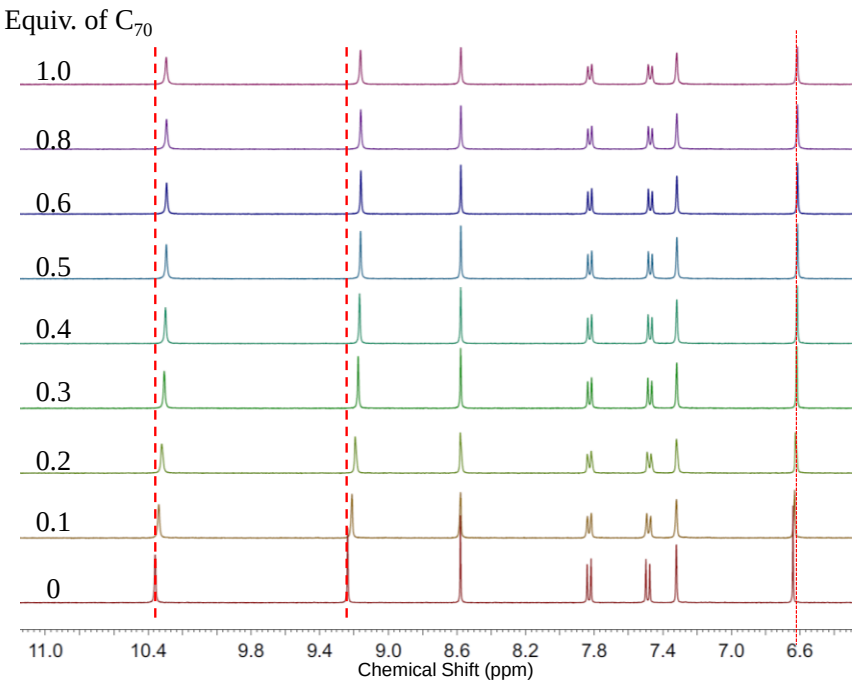

Figure S5. Partial ^{1}H NMR (400 MHz, CD_2Cl_2) spectra for titration of **PTZ1** with C_{70}.

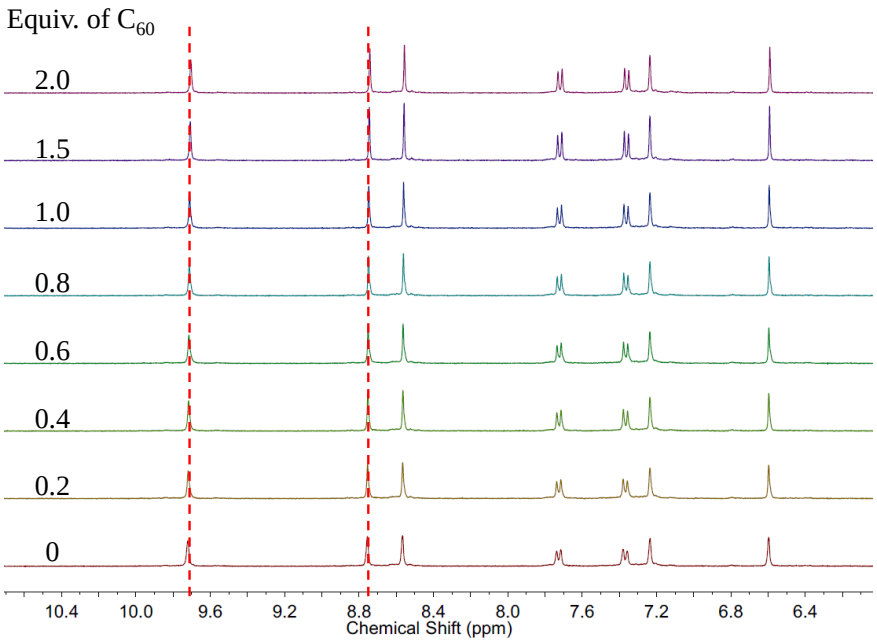

Figure S6. Partial ^{1}H NMR (400 MHz, CD_2Cl_2) spectra for titration of **PTZ2** with C_{60}.

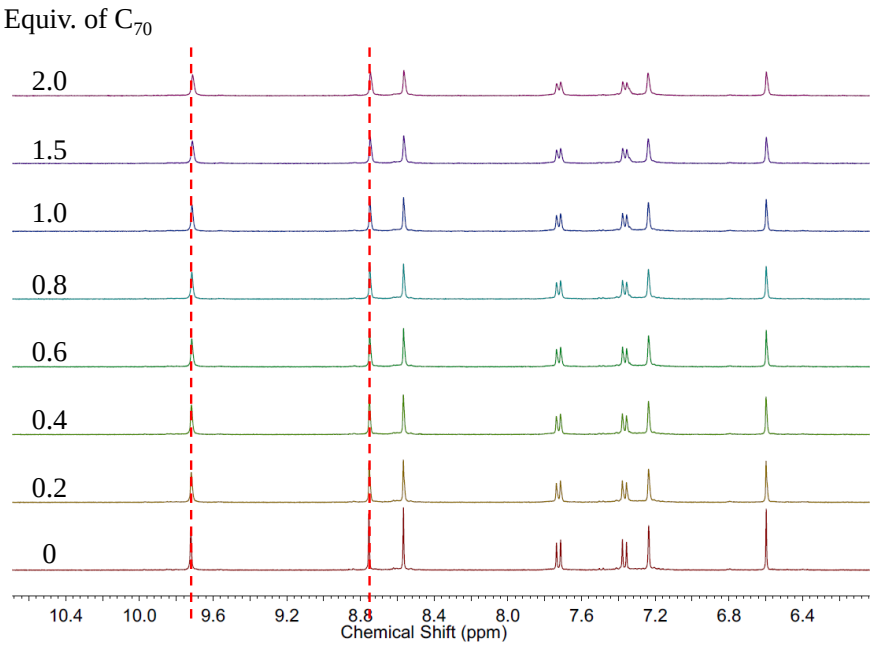

Figure S7. Partial ^{1}H NMR (400 MHz, CD_2Cl_2) spectra for titration of **PTZ2** with C_{70}.

Binding constant Ka in CH_2Cl_2.

To determine the binding constants between fullerene and heterocycloarenes, the change in the chemical shift of protons located lowest field was monitored. The data can be fitted by using the non-linear curve fitting based on the equation:[6]

$$\Delta F_{\text{obs}} = \frac{k_{\Delta\text{HG}}[\text{G}]K_{11}[\text{H}] + 2k_{\Delta\text{H}_2\text{G}}[\text{G}]_0K_{11}K_{21}[\text{H}]^2}{1 + K_{11}[\text{H}] + K_{11}K_{21}[\text{H}]^2}$$

ΔF_{obs} = changes of fluorescence intensity on titration,

$k_{\Delta HG}$ and $k_{\Delta H2G}$ = proportional constants for 1:1 and 2:1 complex,

[H] and [G] = total concentrations of the host and guest,

K_{11} and K_{21} = binding constants for the 1:1 and 2:1 equilibria.

The binding constants were determined by using the program of Pall Thordarson (http://supramolecular.org). The program is freely available and is based on Python using the above equation of the 2:1 equilibrium.

Table S2. Association constants (Ka) of **PTZ1** with fullerenes.

Compound	Fullerene	K_{11} (M^{-1})	K_{21} (M^{-1})	Ka(M^{-2})
PTZ1	C_{60}	1.24	6.66×10^{6}	8.26×10^{6}
	C_{70}	17.34	9.29×10^{5}	1.61×10^{7}

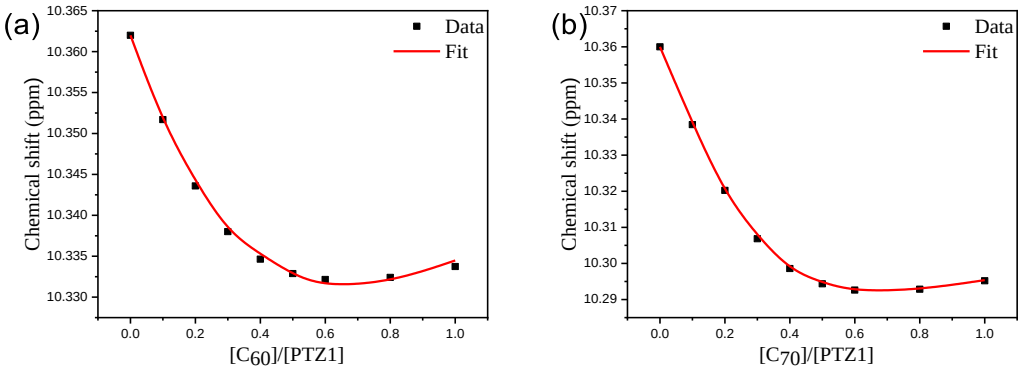

Figure S8. Fitting binding isotherm using a 2:1 association model for the titration of heterocycloarenes **PTZ1** with (a) C_{60} and (b) C_{70}. The change in the chemical shift for proton H_a.

Fullerene binding fluorescence titration studies.

Fluorescence titrations were carried out by adding stock toluene solutions of C_{60} (1.5×10^{-3} M) and C_{70} (1.5×10^{-3} M) to the solution of **PTZ1** (1.0×10^{-5} M), respectively. The binding constants were determined by using nonlinear least-squares curve fitting procedure performed with the online software Bindfit on http://supramolecular.org/ website with a 2:1 global fitting model (Nelder-Mead method).

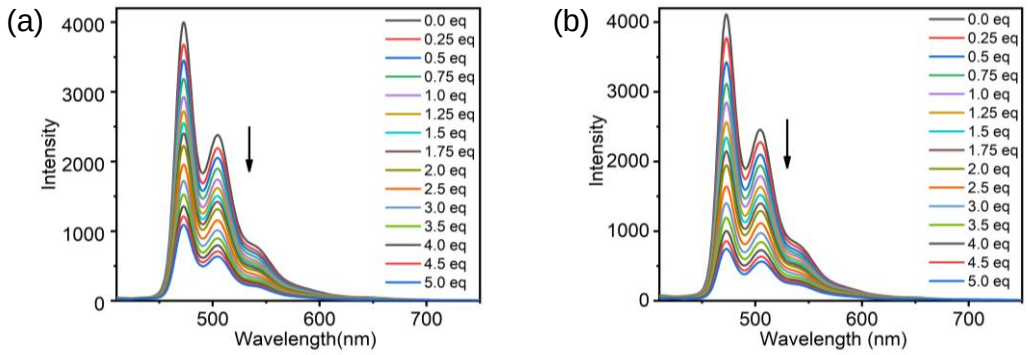

Figure S9. Change of the fluorescence spectrum of **PTZ1** upon gradual addition of C_{60} (a) and C_{70} (b) in toluene.

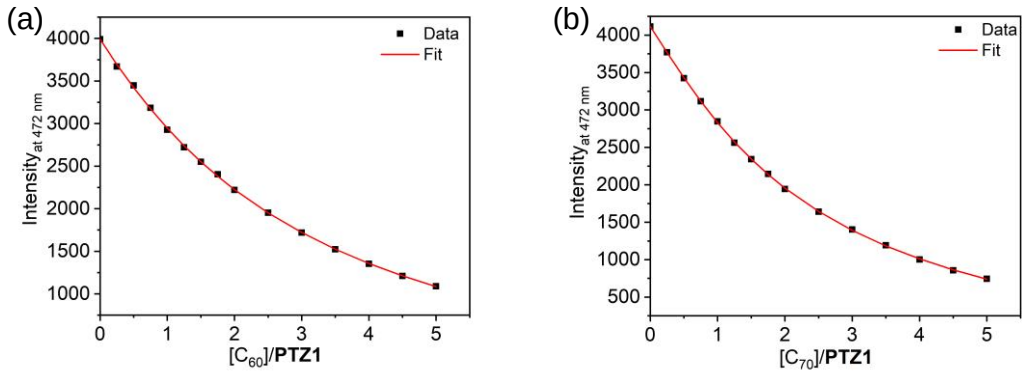

Figure S10. Plot of fluorescence changes at 472 nm versus [C_{60}] (c) and [C_{70}] (d) in toluene for obtaining Ka.

Table S3. Association constants (Ka) of **PTZ1** with fullerenes calculated by fluorescence titration experiments.

Method	**Fullerene**	**K_{11} (M^{-1})**	**K_{21} (M^{-1})**	**Ka(M^{-2})**
Fluorescence Titration	C_{60}	4.7×10^{4}	4.7×10^{3}	2.21×10^{8}
	C_{70}	8.9×10^{4}	2.6×10^{4}	2.31×10^{9}

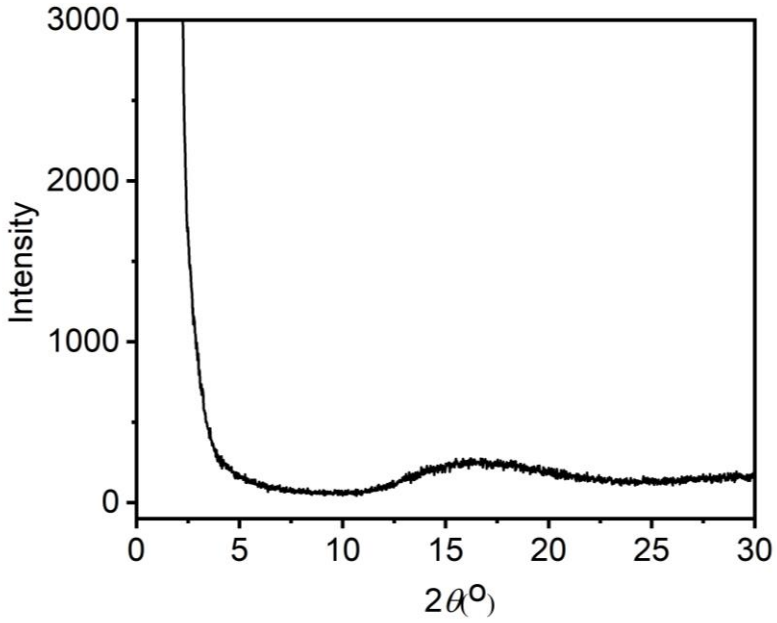

Figure S11. XRD pattern of the spin-coating thin film of compound **PTZ1**. X-ray diffraction was recorded on an X-ray diffractometer at room temperature using Cu Kα radiation (λ = 1.5418 Å) with a θ-2θ configuration.

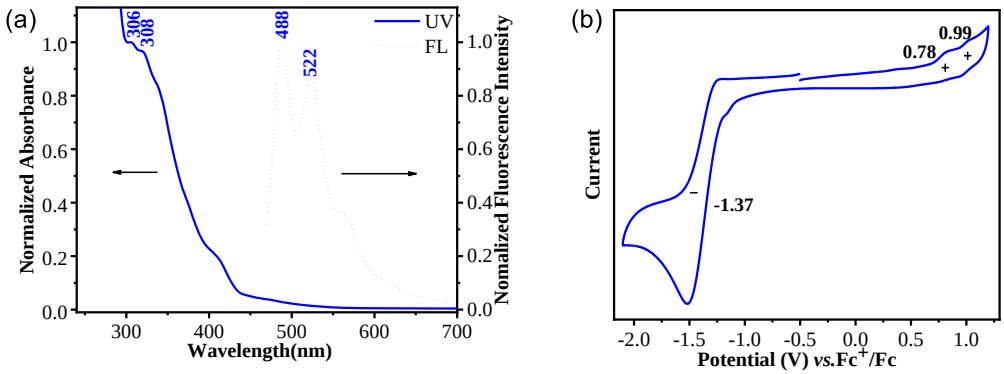

Figure S12. Normalized UV-vis absorption and fluorescence spectra of **PTZ1-Oxi** measured in toluene. (b) Cyclic voltammogram of **PTZ1-Oxi** dissolved in dichloromethane.

3. Theoretical calculations

Density functional theory (DFT) calculations were performed with the Gaussian09 program suite[8] with Becke's threeparameter hybrid exchange functionals and the Lee-Yang-Parr correlation functional (B3LYP) employing the 6-31G(d,p) basis set for all

atoms.[9-14] Time-dependent DFT (TD-DFT) calculations were performed under the same level of theory and basis set as solvation of toluene. NICS values were calculated by using the standard GIAO procedure (NMR pop=NCSall)[15] with the assistance of Multiwfn.[16] ACID plot was calculated by using the method developed by Herges.[17] Chemical shift of ^{1}H NMR in chloroform were calculated at the B97-2/pcSseg-1 level of theory.[18]

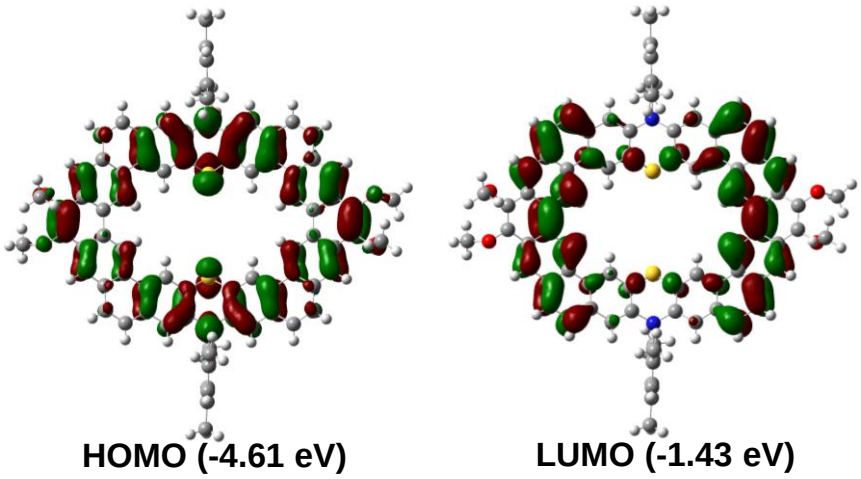

Figure S13. Calculated frontier orbitals and energy levels of **PTZ1**.

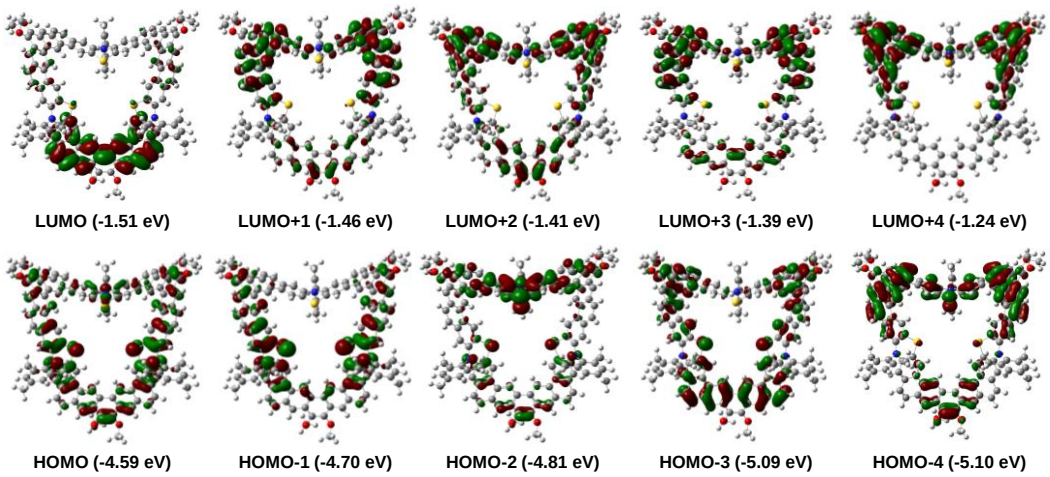

Figure S14. Calculated frontier orbitals and energy levels of **PTZ2**.

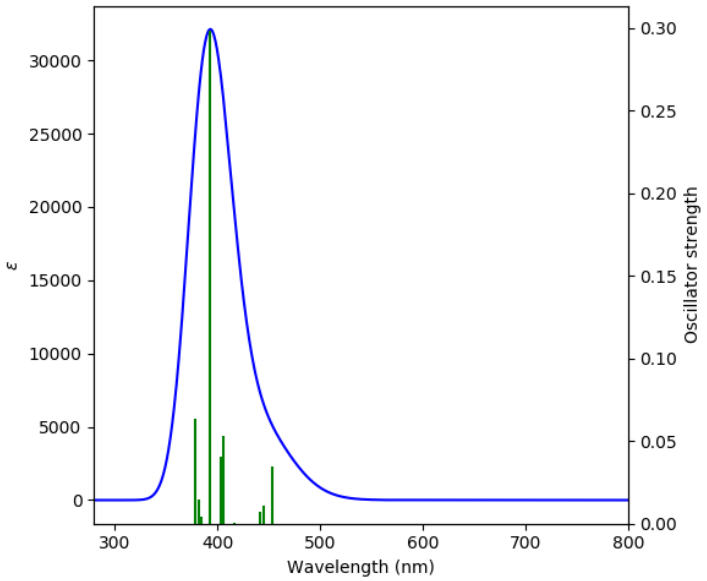

Figure S15. TD-DFT simulated spectrum of **PTZ1** in toluene.

Table S4. Selected TD-DFT (RB3LYP/6-31G(d,p)) calculated energies, oscillator strength and compositions of major electronic transitions of **PTZ1.**

Wavelength(nm)	Osc.Strength(f)	Major contributions
453.2249	0.0349	HOMO->LUMO (89%)
444.6587	0.0107	HOMO->L+1 (53%), HOMO->L+2 (38%)
441.6492	0.0069	HOMO->L+1 (33%), HOMO->L+2 (56%)
417.2164	0.0002	H-1->LUMO (91%)
405.4421	0.0531	H-1->L+1 (60%), H-1->L+2 (24%)
403.3974	0.0402	H-1->L+1 (23%), H-1->L+2 (58%)
392.9395	0.2985	H-1->L+1 (11%), HOMO->L+3 (62%)
384.9126	0.0039	H-2->LUMO (65%)
381.713	0.0145	H-4->L+1 (12%), H-3->LUMO (76%)
378.4621	0.0634	H-3->L+2 (13%), H-2->L+1 (57%)

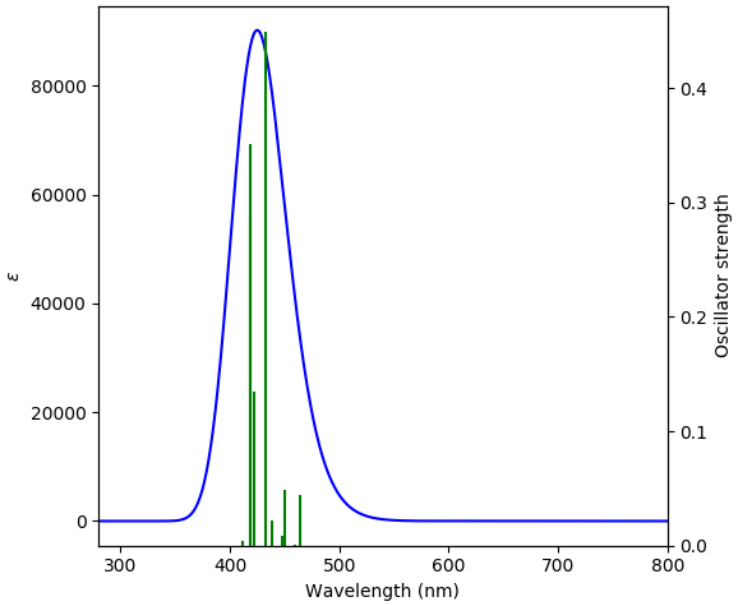

Figure S16. TD-DFT simulated spectrum of **PTZ2** in toluene.

Table S5. Selected TD-DFT (RB3LYP/6-31G(d,p)) calculated energies, oscillator strength and compositions of major electronic transitions of **PTZ2.**

Wavelength (nm)	Osc.Strength(f)	Major contributions
464.2038003	0.0448	HOMO->LUMO (80%)
459.4048948	0.0013	H-1->LUMO (21%), HOMO->L+1 (60%)
449.8864001	0.0485	HOMO->L+2 (75%)
447.4509835	0.0086	H-1->L+1 (27%), HOMO->L+3 (55%)
438.8354972	0.0218	H-1->LUMO (64%), HOMO->L+1 (12%)
432.5130573	0.4496	H-1->L+2 (53%), HOMO->L+4 (22%)
421.7005987	0.1352	H-2->L+1 (14%), H-2->L+2 (26%), H-1->L+3 (28%), HOMO->L+5 (22%)
418.596823	0.2904	H-2->LUMO (10%), H-2->L+1 (12%), H-1->L+1 (33%), HOMO->L+3 (10%)
418.1873752	0.3507	H-2->L+1 (41%), H-1->L+1 (10%), HOMO->L+5 (12%)
411.6751104	0.0036	H-2->LUMO (41%), H-2->L+3 (13%), HOMO->L+3 (20%)

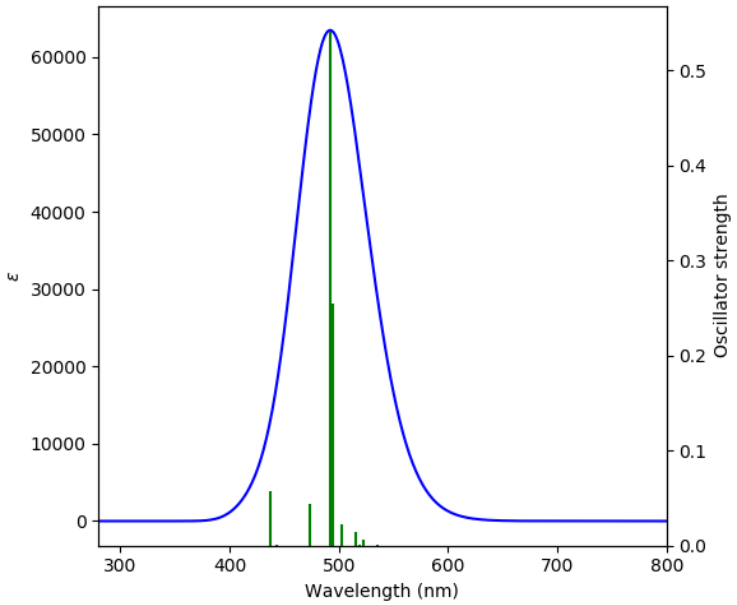

Figure S17. TD-DFT simulated spectrum of **PTZ1-Oxi** in toluene.

Table S6. Selected TD-DFT (RB3LYP/6-31G(d,p)) calculated energies, oscillator strength and compositions of major electronic transitions of **PTZ1-Oxi.**

Wavelength (nm)	Osc.Strength(f)	Major contributions
535.2914	0.0011	HOMO->LUMO (93%)
522.1266	0.0059	H-5->LUMO (26%), H-5->L+1 (36%), H-2->LUMO (11%), HOMO->L+1 (13%)
519.0229	0.0009	H-7->LUMO (20%), H-7->L+1 (14%), H-6->LUMO (29%), H-6->L+1 (15%)
515.7412	0.014	H-5->L+1 (12%), H-2->LUMO (25%), HOMO->L+1 (36%)
502.1839	0.022	H-3->LUMO (34%), H-2->L+1 (41%), HOMO->L+1 (11%)
494.7691	0.2551	H-3->L+1 (11%), H-2->LUMO (24%), H-1->LUMO (16%), HOMO->L+1 (33%)
492.0398	0.5409	H-2->LUMO (10%), H-1->LUMO (82%)
474.1088	0.0439	H-1->L+1 (97%)
443.2915	0.0004	H-3->LUMO (56%), H-2->L+1 (43%)
437.3494	0.0574	H-3->L+1 (76%), H-2->LUMO (21%)

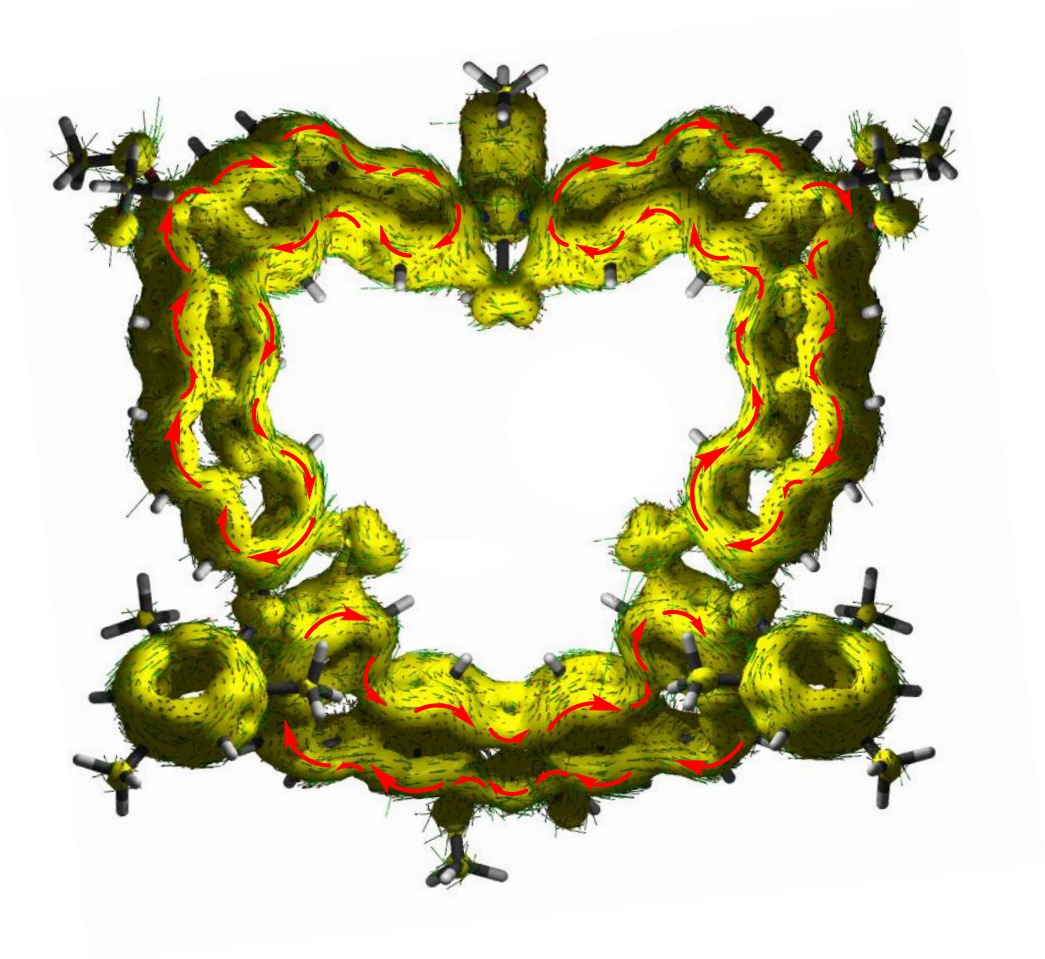

Figure S18. Calculated (RB3LYP/6-31G(d,p)) ACID plot (contribution from π electrons only) of **PTZ2** with isovalues of 0.025. The magnetic field is perpendicular to the XY plane and point out through the paper.

Table S7. Calculated (B97-2/pcSseg-1) and experiment chemical shift of ^{1}H NMR for **PTZ1** and **PTZ1-Oxi** in $CDCl_3$. The distribute of aromatic protons were depend on the calculated results.

PTZ1			**PTZ1-Oxi**		
Aromatic Proton	Chemical Shift (ppm)		Aromatic Proton	Chemical Shift (ppm)	
	Exp.	Cal.		Exp.	Cal.
H_a	10.301	10.852	H_a	9.972	10.221
H_b	9.158	9.561	H_b	10.278	10.366
H_c	8.542	8.956	H_c	8.800	9.110
H_d	7.785	8.107	H_d	7.895	8.210
H_e	7.452	7.632	H_e	7.652	7.857
H_f	7.282	7.632	H_f	7.327	7.653
H_g	6.573	6.724	H_g	7.092	7.284

4. X-ray crystallographic data

Table S8. X-ray crystal data and structure refinement details for **PTZ1** (CCDC 2172358) and **PTZ1-Oxi** (CCDC 2172326).

	PTZ1	**PTZ1-Oxi**
formula	$C_{96}H_{85}N_3O_4S_2$	$C_{80}H_{48}Cl_{16}N_2O_8S_2$
formula wt.	1408.78	1442.02
T (K)	173(2)	173(2)
wavelength (Å)	1.54178	1.54178
crystal size	0.150 × 0.120 × 0.100	0.160 × 0.140 × 0.120
crystal syst.	Monoclinic	Triclinic
space group	P 2_1/c	P-1
a (Å)	20.891(5)	12.745(4)
b (Å)	8.271(3)	14.782(4)
c (Å)	44.433(12)	19.522(4)
α (deg.)	90	82.434(12)
β (deg.)	102.813(10)	83.954(19)
γ (deg.)	90	80.211(17)
V (Å^3)	7487(4)	3579.9(16)
Z/$D_{calcd.}$ (mg/m^3)	4/1.214	2/1.227
μ (mm^{-1})	1.069	3.206
F (000)	2984.0	1480
max / min transmission	0.752/0.594	0.753/0.660

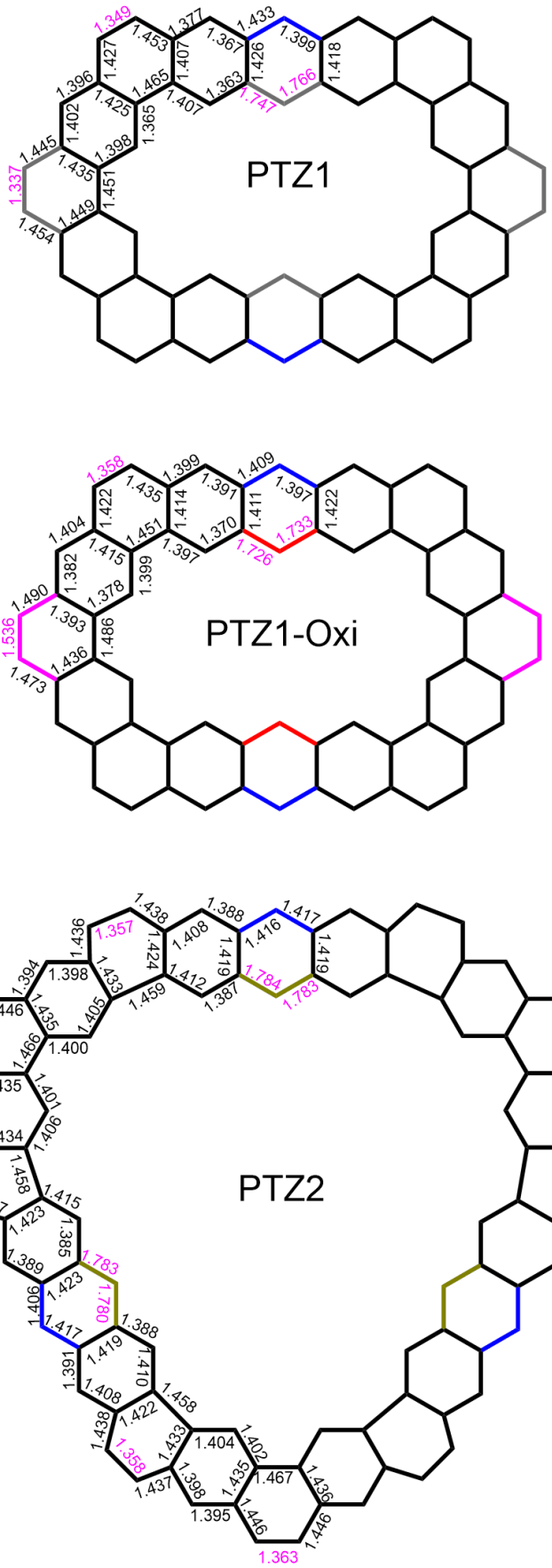

Figure S19. Selected bond lengths (in Å) of **PTZ1**, **PTZ1-Oxi** and **PTZ2**.

5. ^{1}H, ^{13}C NMR and mass spectra of the target compounds

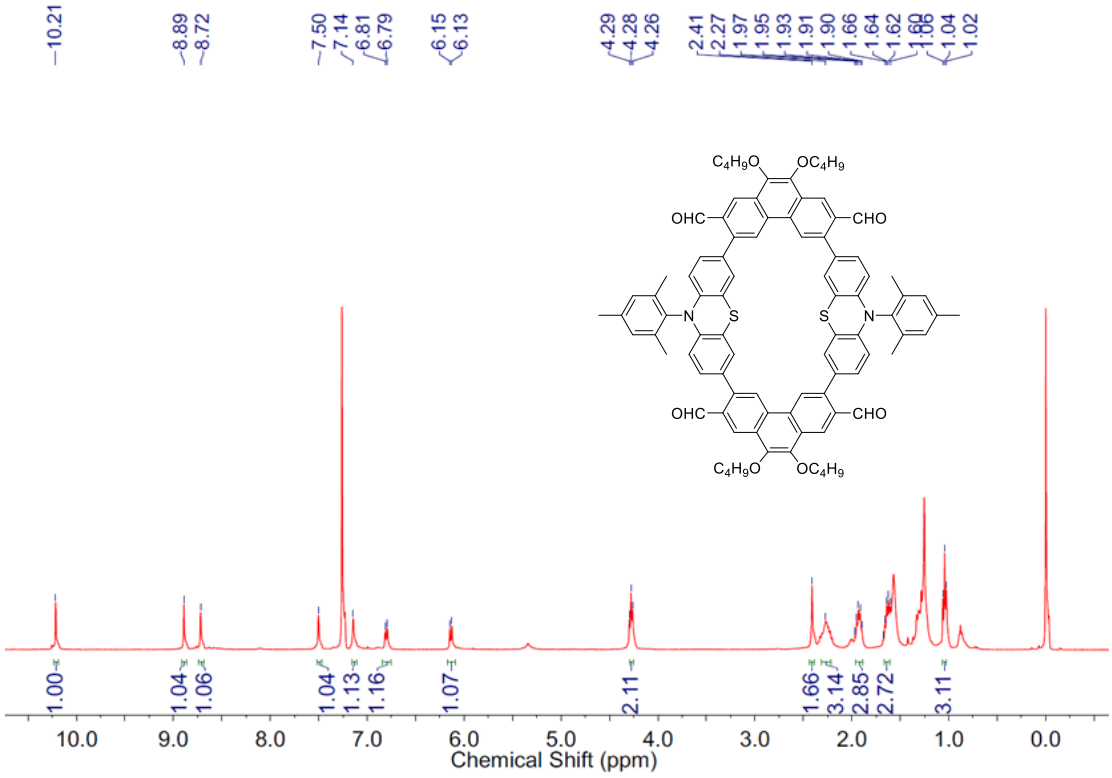

Figure S20. ^{1}H NMR spectrum (400 MHz) of **3a** in $CDCl_3$ at 298 K.

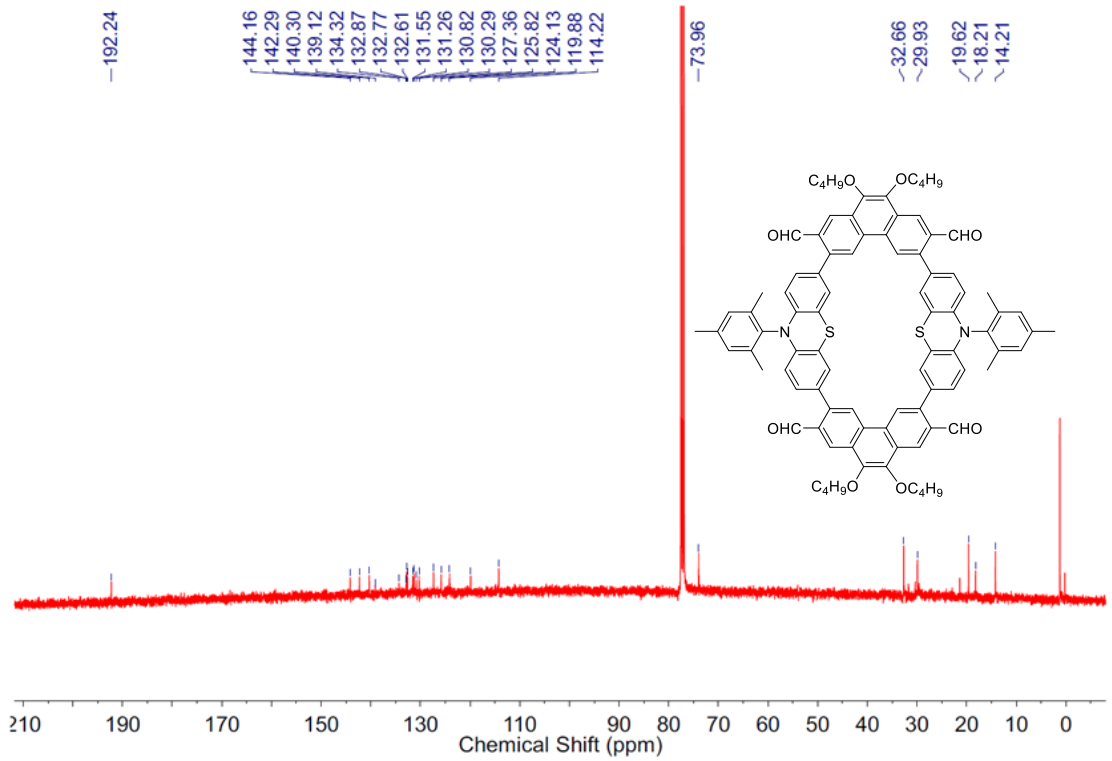

Figure S21. ^{13}C NMR spectrum (101 MHz) of **3a** in $CDCl_3$ at 298 K.

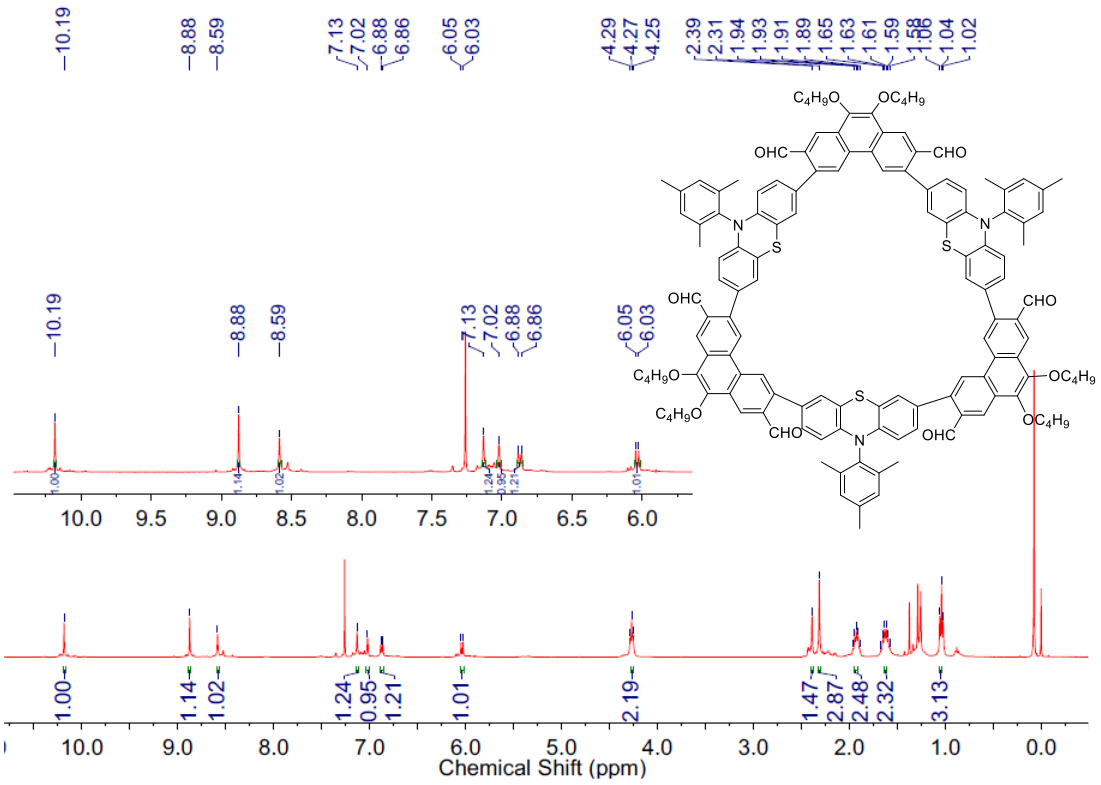

Figure S22. ^{1}H NMR spectrum (400 MHz) of **3b** in $CDCl_3$ at 298 K.

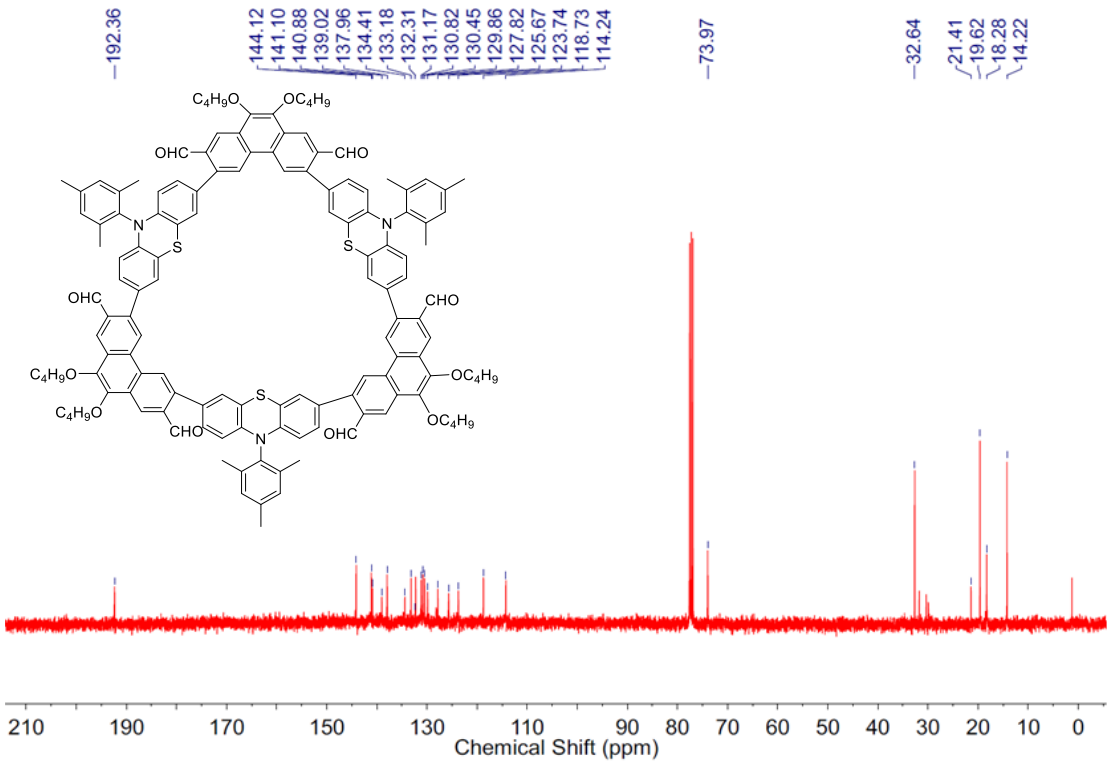

Figure S23. ^{13}C NMR spectrum (101 MHz) of **3b** in $CDCl_3$ at 298 K.

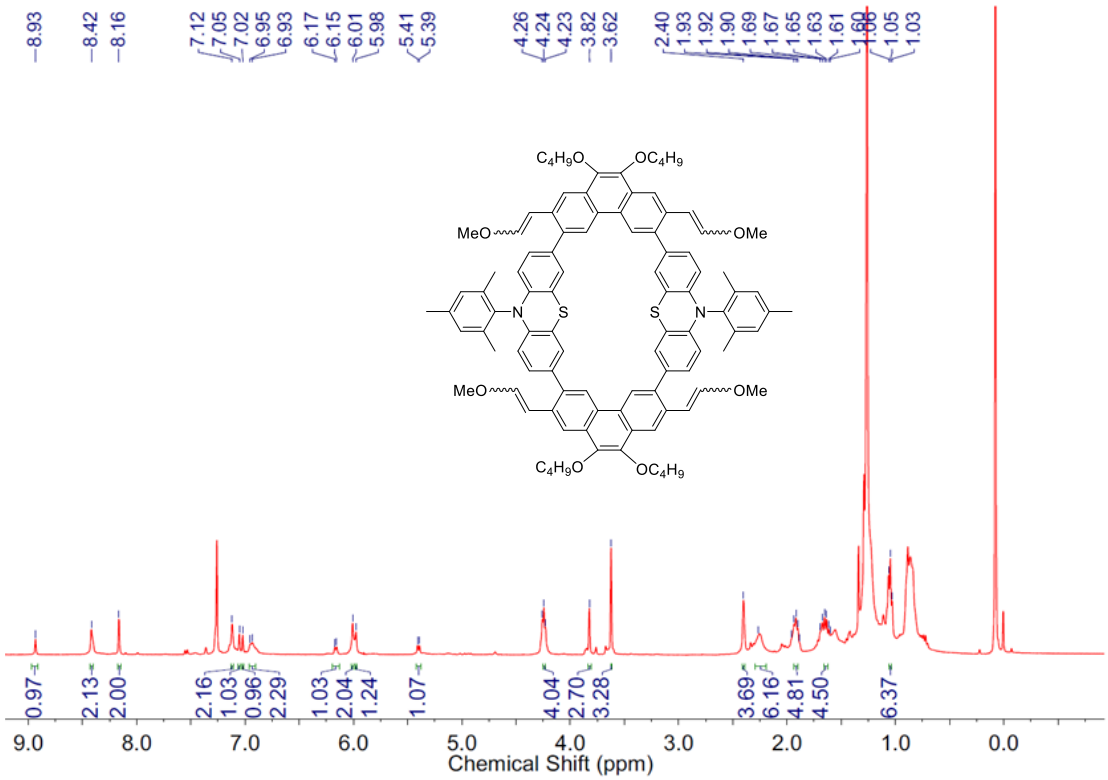

Figure S24. ^{1}H NMR spectrum (400 MHz) of **4a** in $CDCl_3$ at 298 K.

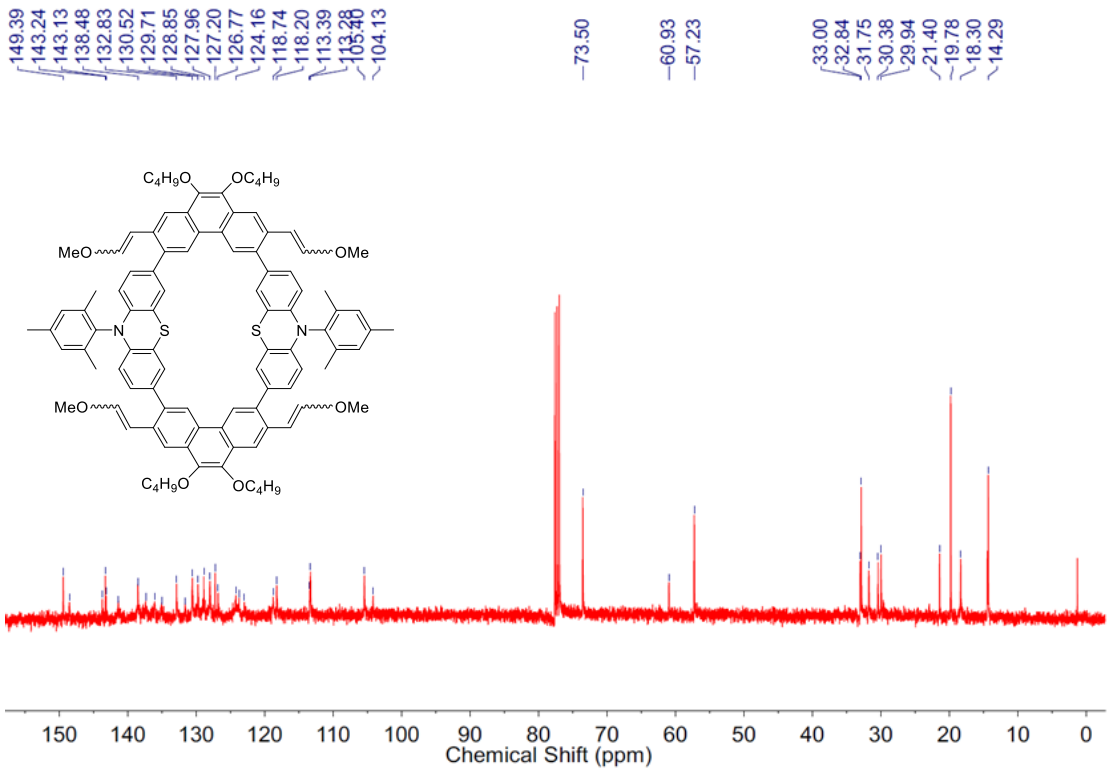

Figure S25. ^{13}C NMR spectrum (101 MHz) of **4a** in $CDCl_3$ at 298 K.

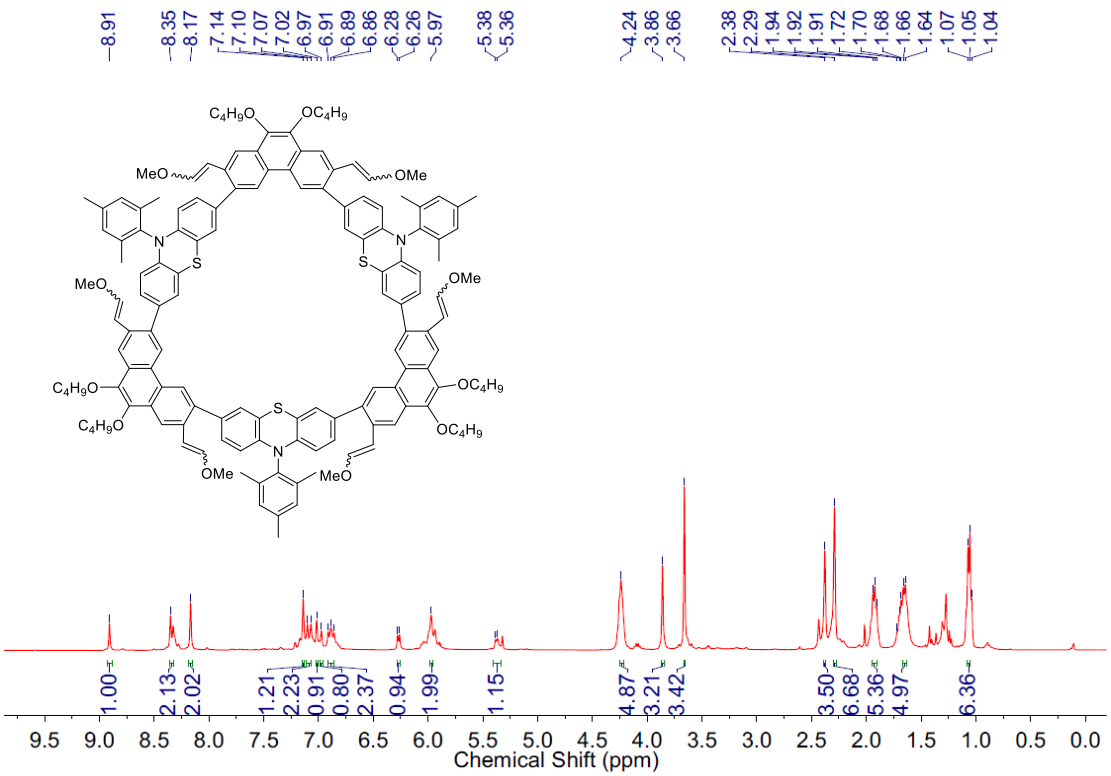

Figure S26. ^{1}H NMR spectrum (400 MHz) of **4b** in CD_2Cl_2 at 298 K.

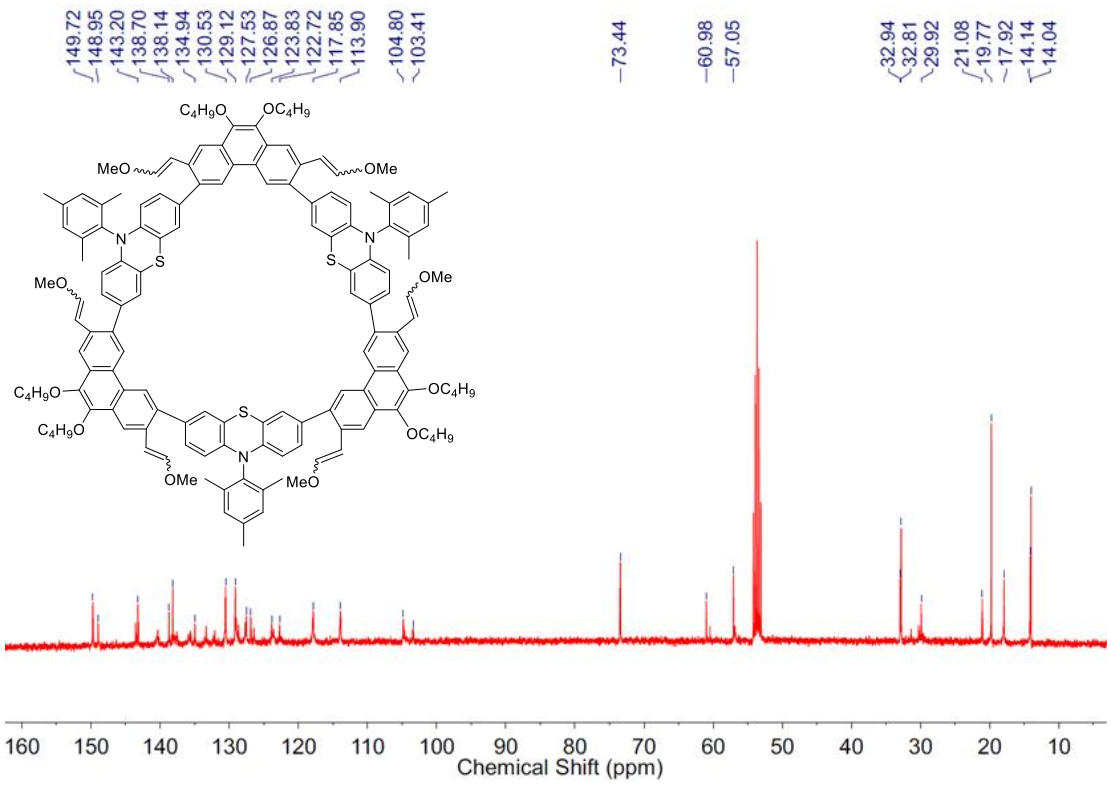

Figure S27. ^{13}C NMR spectrum (101 MHz) of **4b** in CD_2Cl_2 at 298 K.

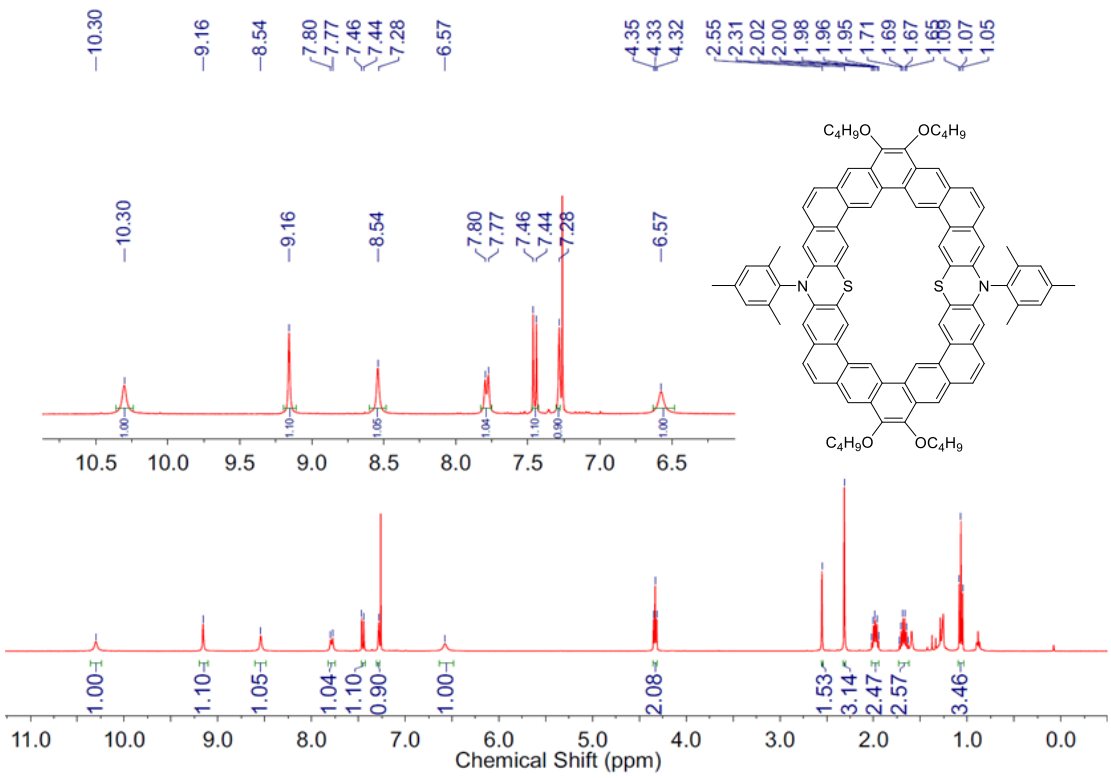

Figure S28. ^{1}H NMR spectrum (400 MHz) of **PTZ1** in $CDCl_3$ at 298 K.

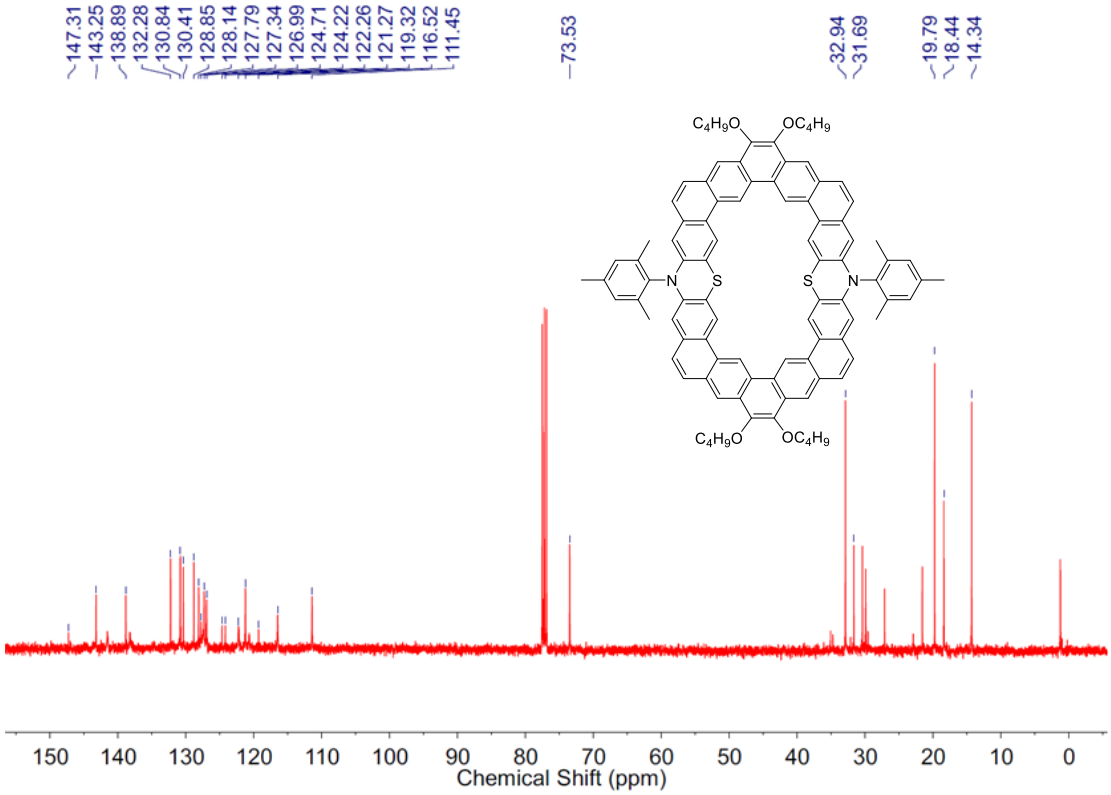

Figure S29. ^{13}C NMR spectrum (101 MHz) of **PTZ1** in $CDCl_3$ at 298 K.

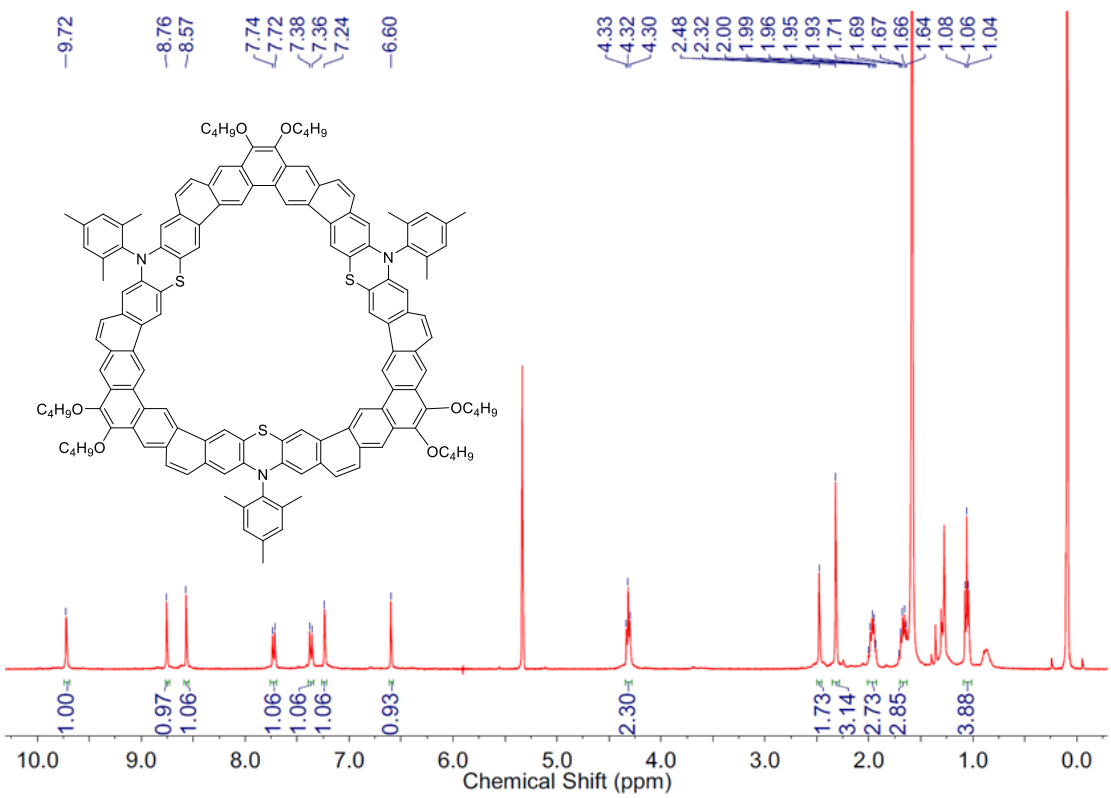

Figure S30. ^{1}H NMR spectrum (400 MHz) of **PTZ2** in CD_2Cl_2 at 298 K.

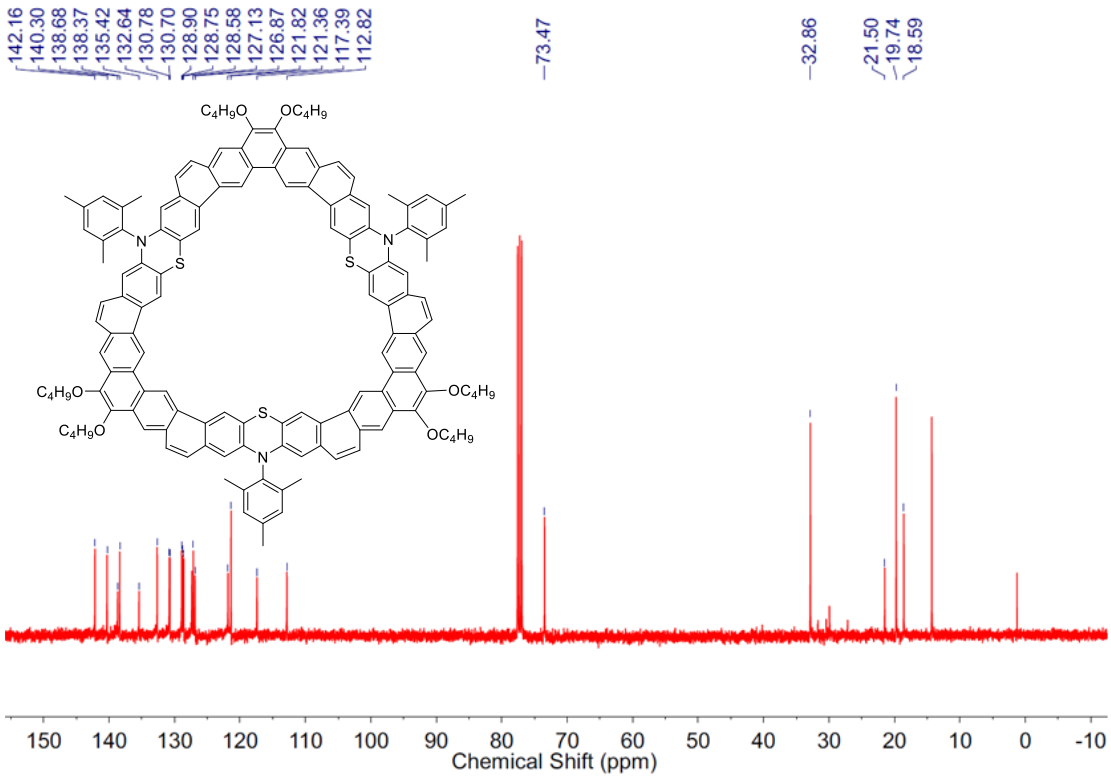

Figure S31. ^{13}C NMR spectrum (101 MHz) of **PTZ2** in $CDCl_3$ at 298 K.

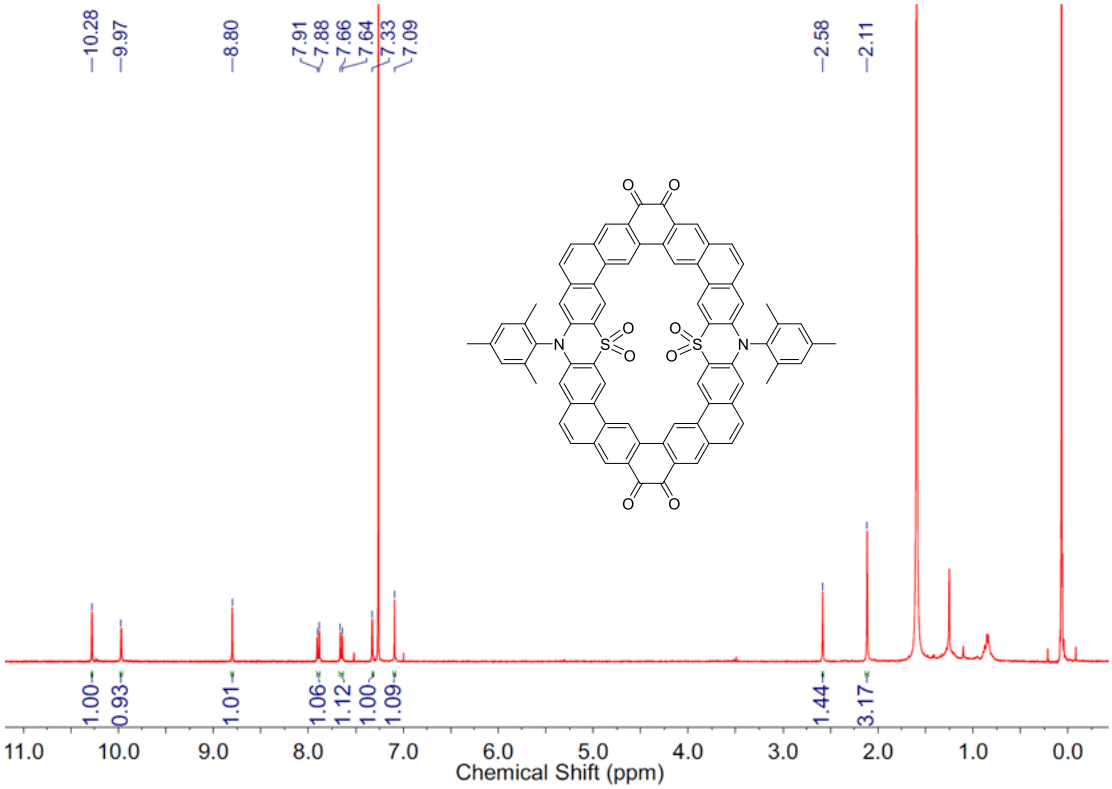

Figure S32. ^{1}H NMR spectrum (400 MHz) of **PTZ1-Oxi** in $CDCl_3$ at 298 K.

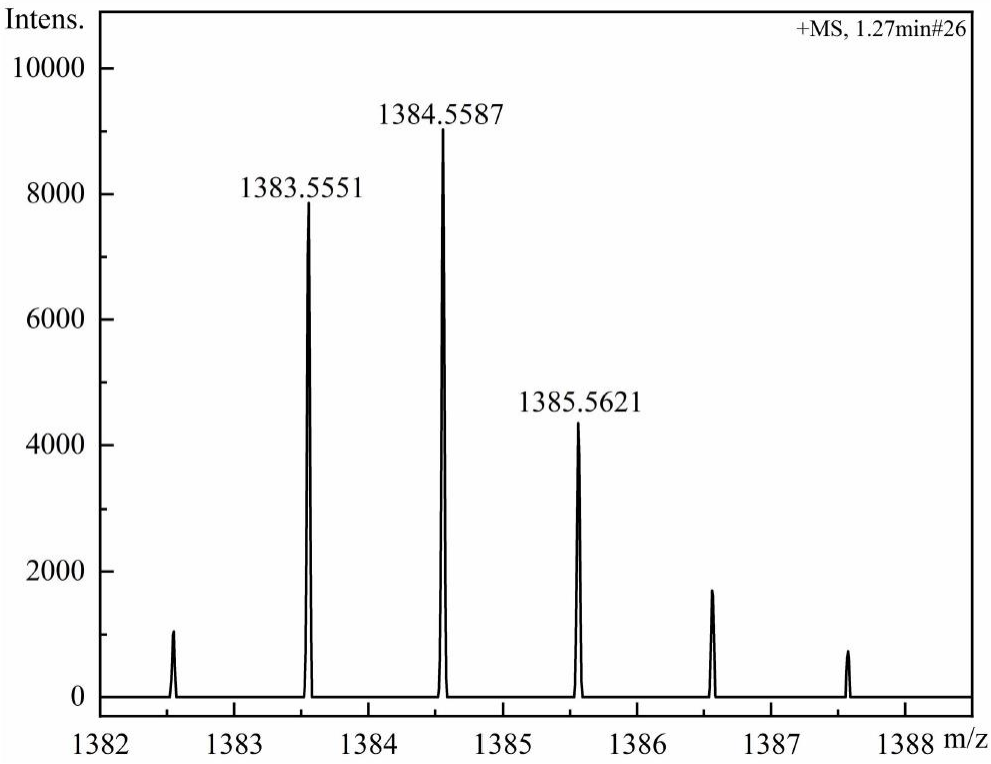

Figure S33. HR mass spectrum (APCI) of **3a**.

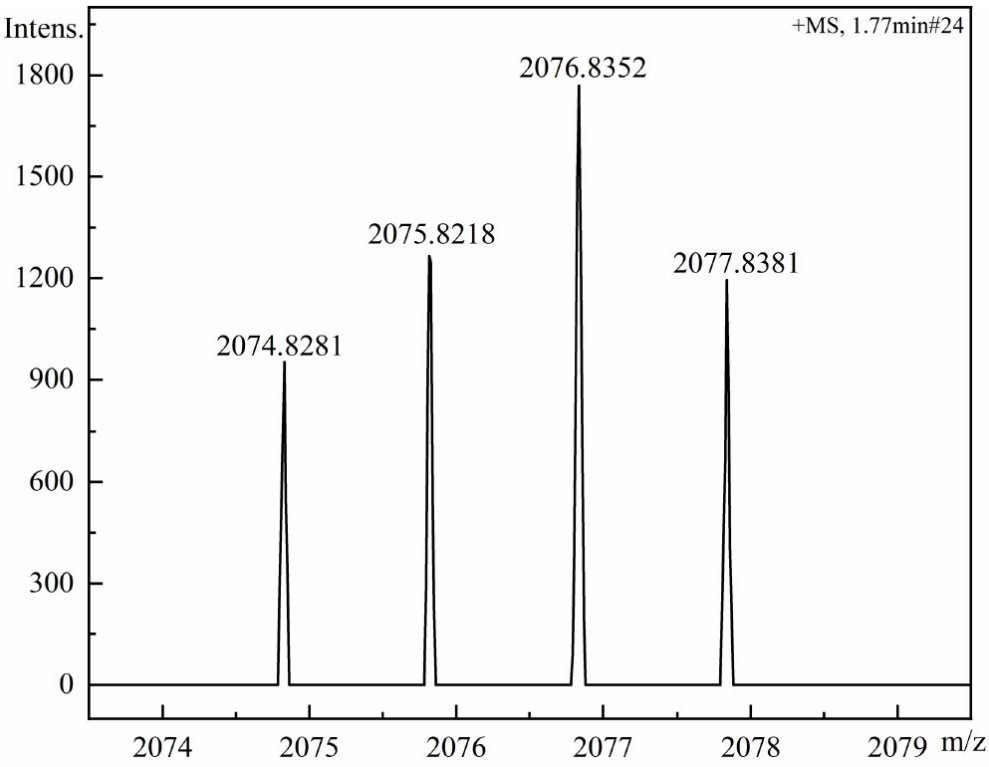

Figure S34. HR mass spectrum (APCI) of **3b**.

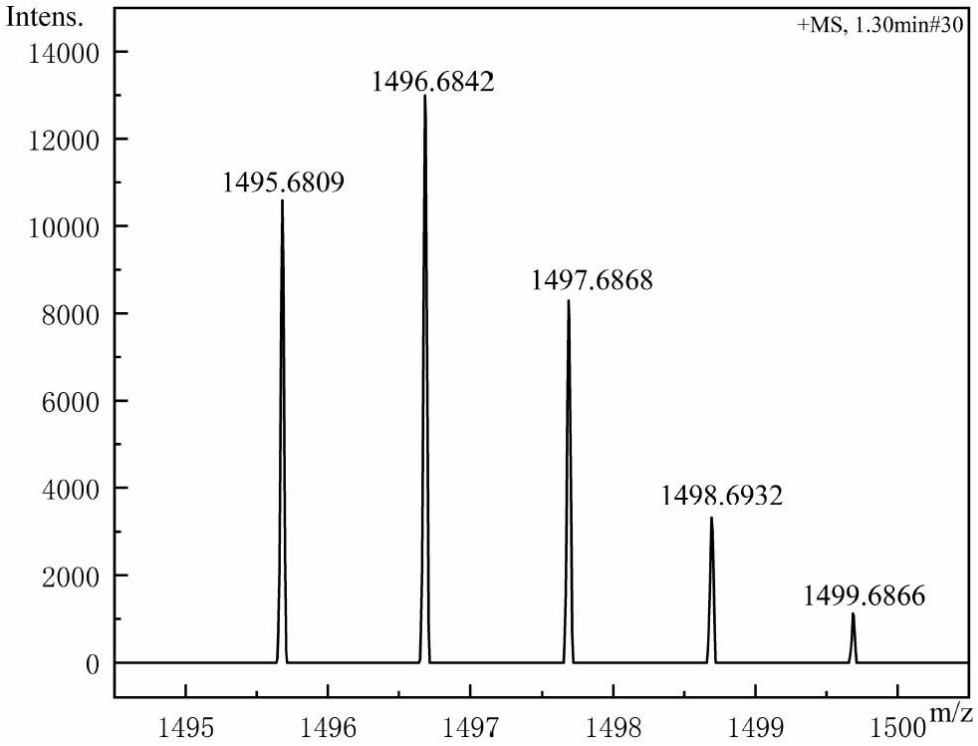

Figure S35. HR mass spectrum (APCI) of **4a**.

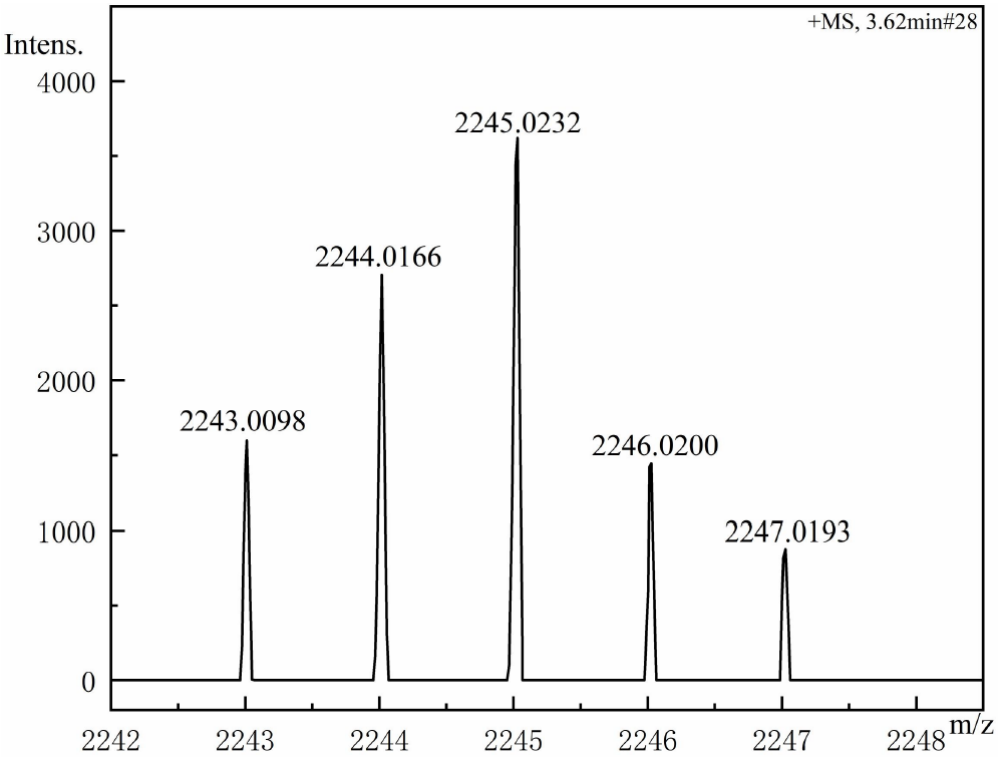

Figure S36. HR mass spectrum (APCI) of **4b**.

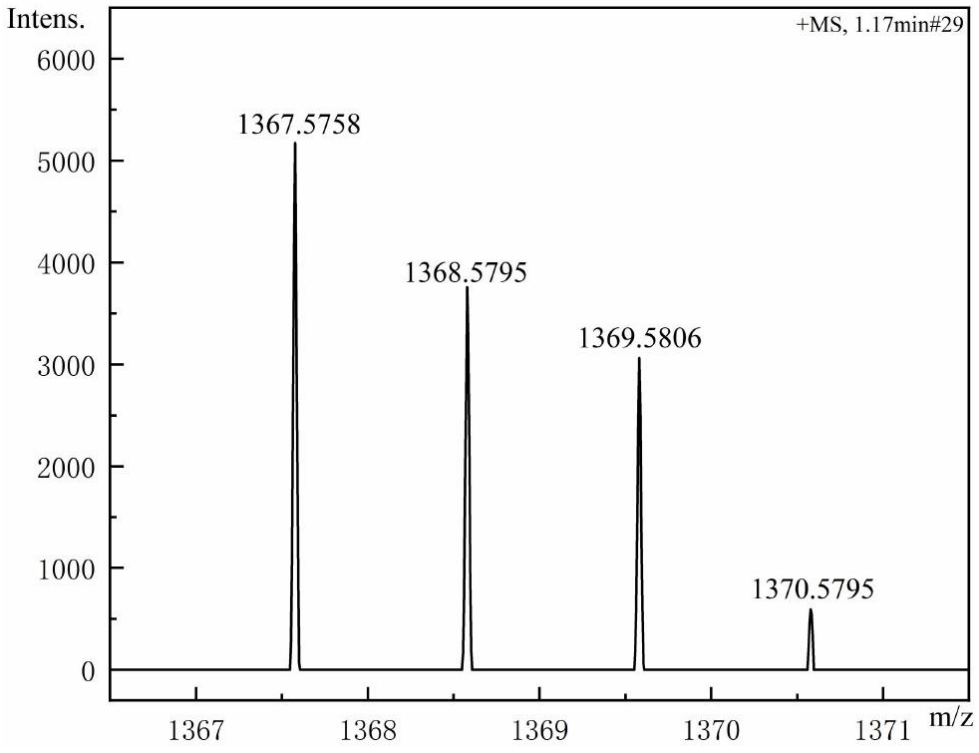

Figure S37. HR mass spectrum (APCI) of **PTZ1**.

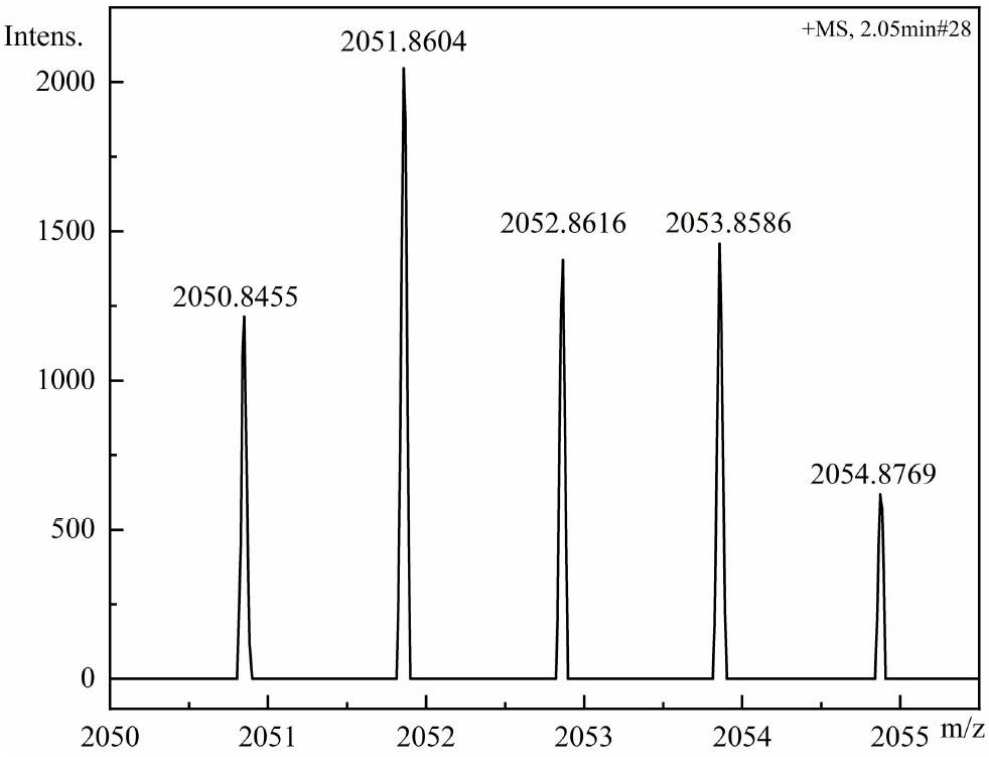

Figure S38. HR mass spectrum (APCI) of **PTZ2**.

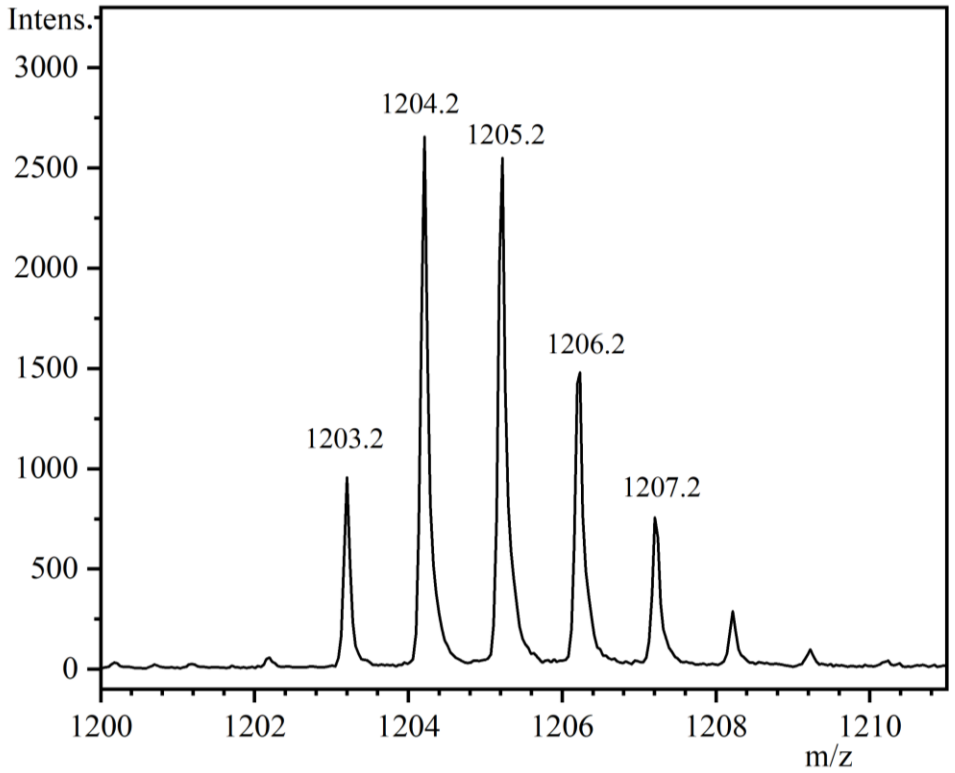

Figure S39. MALDI-TOF Mass spectrum of **PTZ1-Oxi**.

6. Reference

1. Cheng, Y.-J.; Yu, S.-Y.; Lin, S.-C.; Lin, J. T.; Chen, L.-Y.; Hsiu, D.-S.; Wen, Y. S.; Lee, M. M.; Sun, S.-S., A phenothiazine/dimesitylborane hybrid material as a bipolar transport host of red phosphor. *J. Mater. Chem. C* **2016,** *4* (40), 9499-9508.
2. Gregolińska, H.; Majewski, M.; Chmielewski, P. J.; Gregoliński, J.; Chien, A.; Zhou, J.; Wu, Y.-L.; Bae, Y. J.; Wasielewski, M. R.; Zimmerman, P. M.; Stępień, M., Fully Conjugated [4]Chrysaorene. Redox-Coupled Anion Binding in a Tetraradicaloid Macrocycle. *J. Am. Chem. Soc.* **2018,** *140* (43), 14474-14480.
3. Lopez-Garcia, F.; Dong, S.; Han, Y.; Cheng Lee, J. J.; Ng, P. W.; Chi, C., Cyclobis[2,5-(thiophenedimethane)-4,4′-(triphenylamine)] versus Its S,S-Dioxidized Macrocycle: Global Antiaromaticity and Intramolecular Dynamics. *Org. Lett.* **2021,** *23* (16), 6382-6386.
4. Jiménez, V. G.; David, A. H. G.; Cuerva, J. M.; Blanco, V.; Campaña, A. G., A Macrocycle Based on a Heptagon-Containing Hexa-peri-hexabenzocoronene. *Angew. Chem. Int. Ed.* **2020,** *59* (35), 15124-15128.
5. Barendt, T. A.; Myers, W. K.; Cornes, S. P.; Lebedeva, M. A.; Porfyrakis, K.; Marques, I.; Félix, V.; Beer, P. D., The Green Box: An Electronically Versatile Perylene Diimide Macrocyclic Host for Fullerenes. *J. Am. Chem. Soc.* **2020,** *142* (1), 349-364.
6. Thordarson, P., Determining association constants from titration experiments in supramolecular chemistry. *Chem. Soc. Rev.* **2011,** *40* (3), 1305-1323.
7. Brynn Hibbert, D.; Thordarson, P., The death of the Job plot, transparency, open science and online tools, uncertainty estimation methods and other developments in supramolecular chemistry data analysis. *Chem. Commun.* **2016,** *52* (87), 12792-12805.
8. Frisch, M. J.; Trucks, G. W.; Schlegel, H. B.; Scuseria, G. E.; Robb, M. A.; Cheeseman, J. R.; Scalmani, G.; Barone, V.; Mennucci, B.; Petersson, G. A.; Nakatsuji, H.; Caricato, M.; Li, X.; Hratchian, H. P.; Izmaylov, A. F.; Bloino, J.; Zheng, G.; Sonnenberg, J. L.; Hada, M.; Ehara, M.; Toyota, K.; Fukuda, R.; Hasegawa, J.; Ishida, M.; Nakajima, T.; Honda, Y.; Kitao, O.; Nakai, H.; Vreven, T.; Montgomery, J. A.; Jr.; Peralta, J. E.; Ogliaro, F.; Bearpark, M.; Heyd, J. J.; Brothers, E.; Kudin, K. N.; Staroverov, V. N.; Keith, T.; Kobayashi, R.; Normand, J.; Raghavachari, K.; Rendell, A.; Burant, J. C.; Iyengar, S. S.; Tomasi, J.; Cossi, M.; Rega, N.; Millam, J. M.; Klene, M.; Knox, J. E.; Cross, J. B.; Bakken, V.; Adamo, C.; Jaramillo, J.; Gomperts, R.; Stratmann, R. E.; Yazyev, O.; Austin, A. J.; Cammi, R.; Pomelli, C.; Ochterski, J. W.; Martin, R. L.; Morokuma, K.; Zakrzewski, V. G.; Voth, G. A.; Salvador, P.; Dannenberg, J. J.; Dapprich, S.; Daniels, A. D.; Farkas, O.; Foresman, J. B.; Ortiz, J. V.; Cioslowski, J.; Fox, D. J. *Gaussian 09 Rev. C.01*, Gaussian, Inc., Wallingford, CT, 2010.
9. Becke, A. D., Density-functional thermochemistry. III. The role of exact exchange. *J. Chem. Phys.* **1993,** *98* (7), 5648-5652.
10. Lee, C.; Yang, W.; Parr, R. G., Development of the Colle-Salvetti correlation-energy formula into a functional of the electron density. *Phys. Rev. B: Condens. Matter* **1988,** *37* (2), 785-789.
11. Yanai, T.; Tew, D. P.; Handy, N. C., A new hybrid exchange–correlation functional using the Coulomb-attenuating method (CAM-B3LYP). *Chem. Phys. Lett.* **2004,** *393* (1), 51-57.

12. Ditchfield, R.; Hehre, W. J.; Pople, J. A., Self-Consistent Molecular-Orbital Methods. IX. An Extended Gaussian-Type Basis for Molecular-Orbital Studies of Organic Molecules. *J. Chem. Phys.* **1971,** *54* (2), 724-728.
13. Hehre, W. J.; Ditchfield, R.; Pople, J. A., Self-Consistent Molecular Orbital Methods. XII. Further Extensions of Gaussian-Type Basis Sets for Use in Molecular Orbital Studies of Organic Molecules. *J. Chem. Phys.* **1972,** *56* (5), 2257-2261.
14. Hariharan, P. C.; Pople, J. A., The influence of polarization functions on molecular orbital hydrogenation energies. *Theoret. Chim. Acta* **1973,** *28* (3), 213-222.
15. Schleyer, P. v. R.; Maerker, C.; Dransfeld, A.; Jiao, H.; van Eikema Hommes, N. J. R., Nucleus-Independent Chemical Shifts: A Simple and Efficient Aromaticity Probe. *J. Am. Chem. Soc.* **1996,** *118* (26), 6317-6318.
16. Lu, T.; Chen, F., Multiwfn: A multifunctional wavefunction analyzer. *J. Comput. Chem.* **2012,** *33* (5), 580-592.
17. Geuenich, D.; Hess, K.; Köhler, F.; Herges, R., Anisotropy of the Induced Current Density (ACID), a General Method To Quantify and Visualize Electronic Delocalization. *Chem. Rev.* **2005,** *105* (10), 3758-3772.
18. Flaig, D.; Maurer, M.; Hanni, M.; Braunger, K.; Kick, L.; Thubauville, M.; Ochsenfeld, C., Benchmarking Hydrogen and Carbon NMR Chemical Shifts at HF, DFT, and MP2 Levels. *J. Chem. Theory Comput.* **2014,** *10* (2), 572-578.